Nanofabrication of direct positioning atomic force microscope (AFM) probes and a novel method to attain controllable lift-off

by

Shuo Zheng

A thesis
presented to University of Waterloo
in the fulfillment of the
thesis requirement for the degree of
Master of Applied Science
in
Electrical and Computer Engineering (Nanotechnology)

Waterloo, Ontario, Canada, 2017

© Shuo Zheng 2017

Author's Declaration

I hereby declare that I am the sole author of this thesis. This is a true copy of the thesis, including any required final revisions, as accepted by my examiners.

I understand that my thesis may be made electronically available to the public.

Abstract

This thesis focuses on nanofabrication and its applications in the area related to atomic force microscope (AFM) probes and a novel way of constructing the bi-layer system for liftoff. The contribution of this thesis is therefore the introduction and characterization of nanotechnologies and their applications in fabricating the AFM probes (Part 1). Moreover, an introduction of the liftoff and the exhibition of the experimental results of our technique will be provided (Part 2).

The first part of this thesis consists of four chapters. The first chapter brings a brief introduction and an overview of nanotechnologies and nanofabrication to give a big picture of what they are. The second chapter introduces three major nanofabrication techniques that are crucial in manufacturing the AFM tip. Those are evaporation, wet etch and dry etch. The basic concepts, working mechanism and important parameters of these three techniques are discussed. The third chapter presents detail of the AFM probe with its history, principle of operation, fabrication method and carbon nanotube tips. After equipping the knowledge provided in the first three chapters, fabricating a particular direct positioning AFM probe will be discussed next. Therefore, chapter 4 introduces the details of our method to batch fabricate the direct positioning AFM probe step-by-step. Parameters and goals of each step are presented with schematics and SEM images from our results.

The second part of this thesis consists of four chapters as well. The first chapter introduces the essentials of a liftoff process and current popular methods to create moderate undercuts. The second chapter describes the experimental process of our technique to acquire controllable undercut by tuning the ratio of ZEP/PMMA mixture. The third part exhibits the results of contrast curves for various mixtures, undercut profiles and Chromium line arrays produced by our liftoff process.

Acknowledgement

First I would like to thank the support from my families. They always encourage and support me behind the scenes so that I can dedicate myself to the research works.

Gratitude also owes to the nanofabrication facilities at Quantum NanoFab, WATLab and Giga-to-Nanoelectronics (G2N) Laboratory in University of Waterloo. Quantum NanoFab infrastructure would not be possible without the significant contributions of the Canada Foundation for Innovation, the Ontario Ministry of Research & Innovation, Industry Canada and Mike & Ophelia Lazaridis. And G2N laboratory is funded by Canada Foundation for Innovation, the Ontario Ministry of Research & Innovation and Industry Canada. Their supports are always grateful.

Also, I'd like to thank the priceless guidance and suggestions from my supervisor Professor Bo Cui. He turned me from someone who has literally zero knowledge of nanotechnologies into an eligible candidate for a Master Degree of Science specified in Nanotechnology.

Table of Contents

List of Figures vii

List of Tables xii

(Part 1)

Chapter 1 Introduction.. 1

1.1 What is nanotechnology? 1

1.2 Overview of nanofabrication 2

Chapter 2 Specific techniques for AFM probe fabrication... 5

2.1 Evaporation 5

2.2 Etching 9

2.2.1 Wet etch 11

2.2.2 Dry etch 14

Chapter 3 Introduction of Atomic Force Microscope Probe Fabrication 19

3.1 History 19

3.2 Probe structures and characters 20

3.3 Principle of operation 21

3.4 Fabrication methods 22

3.4.1 Indirect method 23

3.4.2 Direct method 27

3.4.3 Sharpening of the tips 29

3.5 Future of the AFM probe --- carbon nanotube tips 30

3.6 Conclusion 33

Chapter 4 Batch fabrication of Direct Positioning (DP) AFM tip.. 35

4.1 Shape of AFM tips 35

4.2 Fabrication of DP AFM tip 37
4.2.1 Electron-beam evaporation of aluminum 38
4.2.2 Deep Si RIE (DRIE) 41
4.2.3 Al wet etch 42
4.3 Conclusion 44

(Part 2)

Chapter 5 Mixture of ZEP and PMMA with varying ratios for tunable sensitivity as a lift-off resist with controllable undercut 48

5.1 Introduction 48
5.2 Experimental 51
5.3 Results and discussions 51
5.3.1 Contrast curves 52
5.3.2 Resist profile and lift-off of thick Cr 53
5.4 Conclusions 56

References........ 57

List of Figures

Figure 1.1 Sizes of different objectives in nanometers (Picture courtesy to the National Cancer Institute). 1

Figure 1.2 The schematic of the (a) top-down and the (b) bottom-up approach. In the top-down approach, the resist is first patterned by lithography, and then (1) the pattern is transferred by deposition followed by liftoff, or (2) the pattern is transferred by direct etching. In the bottom-up approach, the pattern is usually acquired by self-assembly and then transferred into substrate by liftoff. 2

Figure 2.1 The picture of a modern evaporator for R&D purpose. (Picture courtesy to the Intlvac Thin Film Corporation) 5

Figure 2.2 The schematic of (a) thermal evaporation and (b) electron-beam evaporation. (Courtesy to Hivatec Laboratory). 6

Figure 2.3 An example of the shadowing problem that may occur during the evaporation. 9

Figure 2.4 A graphical representation of (a) a poor selectivity causes the etchant to attack the bottom layer material while removing the top layer, (b) a high selectivity causes etch out the top layer without affecting the underlying layer. (Courtesy to Smack.) 10

Figure 2.5 A schematic of (a) isotropic etching that has equal etching rate in all direction, and (b) anisotropic etching for which the etching rate is slower in <111> planes. 10

Figure 2.6 An illustration of wet etch process. Reactants first diffuse to the surface of the film to be etched. Then reactions are going to take place. Lastly, the products of the reaction diffuse away by the liquid flow in the solution of the etchant. 11

Figure 2.7 A graphical illustration of three major planes in a cubic unit silicon. 12

Figure 2.8 An illustration of a V-shaped groove and a U-shaped groove. 13

Figure 2.9 A table of wet etchants for some common nanofabrication materials. (Contents courtesy to Wikipedia) 14

Figure 2.10 A schematic of the structure in a plasma. (Courtesy to Henrik Obst) 15

Figure 2.11 Reaction steps of RIE for the case of Si etching by using CF4. 16

Figure 2.12 The graph compares the achievable etch rated by XeF_2 gas only, Argon ion plasma only and the combination of them. The combination of chemical and physical etch, namely ion-assisted chemical etch significantly improves the efficiency of the etching. 17

Figure 3.1 (a) Experimental setup of Binnig, Quate and Gerber's first AFM. (b) Its dimension. The STM and AFM piezoelectric drives are facing each other, sandwiching the diamond tip that is glued to the lever. (c) The picture of the first AFM instrument (image copyright Science Museum London/SSPL). 20

Figure 3.2 Schematic of a normal AFM probe and its dimensions. (Picture courtesy to Oliver Krause) 20

Figure 3.3 Description of the operation of the AFM. (a) Tip follows contour B to maintain constant force between tip and sample. Brief schematic of AFM operations by measuring (b) cantilever deflection (c) sample movement in z-direction. 22

Figure 3.4 Image of commercial (a) 4-inch wafer with 380 probes, (b) 6-inch wafer with more than 1000 probes, (c) close look of tips on the wafer. (Picture courtesy to Oliver Krause) 22

Figure 3.5 Fabrication steps of regular nitride probes. (a) thermal oxidation to coat oxide on both sides of silicon wafer (<100> orientation), (b) photolithography to expose resist, (c) resist development, (d) spin coating of protection resist on back side and etch oxide with BHF, (e) remove resist with acetone/isopropanol, (f) KOH wet etch to remove Si, (g) remove oxide with BHF, (h) grow oxide, deposit nitride, remove them on the backside, and spin-coat photoresist, (i) photolithography to expose the resist, (j) develop the resist and etch oxide then nitride, (k) dice Pyrex wafer (to be used as a handle), (l) anodic bonding the nitride and the Pyrex wafer, (m) dice and remove unnecessary portion of Pyrex, (n) KOH wet etch to remove Si, and (o) BHF etch to remove the oxide layer. 24

Figure 3.6 Schematic of the etching of mold by (a) RIE only and (b) a combination of RIE and KOH.[9] 26

Figure 3.7 Fabrication process to make probe by molding scheme. (1) Prepare tip area by selectively etching of silicon with KOH solution. The pit and flat surfaces were grown with thermal silicon dioxide and finally coated with copper. (2) Grow a continuous layer of graphene on copper film by CVD method. (3) Coat a thin SU-8 resist to fill the tip mold and; expose and develop to define the cantilever. (4) Argon dry etch to remove the graphene elsewhere where there was no SU-8 film. Later, process a second and thick SU-8 to pattern the probe body. (5) After removal of silicon dioxide with HF solution, silicon with KOH and Cu with wet etchant, probe was released with graphene layer.[10] 27

Figure 3.8 Fabrication steps of regular silicon probe. (a) Start with Si wafer, (b) next, coat SiO2 on both sides of silicon wafer (<100> orientation), (c) then, coat photoresist on back side of wafer and photolithography (exposure of the photoresist through a chromium/quartz mask) to define the cantilever back shape, (d) next, develop the exposed photoresist, (e) deposit photoresist in front side of the sample

and photolithography to shape the cantilever top side, (f) development of the exposed photo resist, (g) isotropic wet etch to remove the silicon dioxide, (h) next, dissolve the photo resist, (i) anisotropic wet etch with KOH to remove silicon. The formation of the tip is finished when the "oxide shield" falls off, (j) isotropic wet etch to remove silicon dioxide and then deposit the silicon nitride layer to protect the tip side of the probe, (k) next, anisotropic KOH wet etch to remove silicon from back side. The thickness of the cantilever is determined during this step, (l) finally, isotropic wet etch to remove the silicon nitride. 28

Figure 3.9 Oxidation sharpening process (Courtesy to Nanosensor). 30

Figure 3.10 (a) The structure of a single-walled carbon nanotube. Each vertex corresponds to a sp2-bonded carbon atom. (b) SEM image of an AFM probe with a CNT tip. 31

Figure 3.11 The pore-growth technique for CVD nanotube tip production: The panels on the left illustrate the steps involved in tip production: flattening, pore formation, catalyst deposition, and CVD nanotube growth. SEM (top right, 1mm scale bar) and TEM (bottom right, 20nm scale bar) of individual carbon nanotube tips produced by the pore growth method. 32

Figure 3.12 Surface growth method for CVD nanotube tip preparation: (a) Schematic illustration of surface growth process, where nanotubes grow on the pyramidal surface, guided along the edges towards the tip apex. (b) SEM and (c) TEM images of a single-walled nanotube surface growth tip consisting of two single-walled nanotubes. 33

Figure 4.1 SEM images of tips with different shapes, (a) 4-side pyramidal tip (b) 3-side pyramidal tip (c) high aspect ratio tip (d) sphere-end tip. (SEM pictures courtesy to Nano Sensors, Nanotools, Nano World) 36

Figure 4.2 The SEM image of a corner-like DP tip made by our process. 37

Figure 4.3 A picture of the probe captured by the built-in camera of Veeco AFM system. The cross mark refers only an approximate location of the tip. 37

Figure 4.4 A schematic of angled deposition of aluminum. The blue areas represent the AFM tip and the red areas show the surface that will be covered by aluminum. (a) If aluminum is deposited in this direction (“front deposition”), little aluminum will be deposited on the outer side of the tip, (b) shadowing areas occur both on the cantilever and the inner sidewall of the tip once aluminum is deposited in this direction (“reverse deposition”). 38

Figure 4.5 Actual setting in the deposition system. A stub of 60° is used to provide an angle so that the depositions described in Figure 4.4 (a) and (b) are carried out respectively. 39

Figure 4.6 The SEM images compare the results of protective layer consisting of (a) Cr, (b) Al. It is clearly to see that large stresses distort the Cr layer and the unprotected regions of silicon are damaged during RIE in the next step. On opposite, Aluminum is competent to keep tip well-protected. 40

Figure 4.7 SEM images of (a) "front deposition" achieved on an ACT tip, clear edge of Al is observed and (b) "reverse deposition" on a 3-sided pyramid tip, clear shadowing area is shown. 41

Figure 4.8 SEM images for the etch results of (a) ACT tip that has undergone "front deposition" and (b) 4-sided pyramid tip that has undergone "reverse deposition". 42

Figure 4.9 SEM images of (a) AFM tips with incomplete HF wet etch, clear Al residue can be observed, (b) tips with clean and sufficient HF wet etch. 44

Figure 4.10 An image of the backside of a tip made by our process captured by the built-in camera. There is a clear vacancy on the cantilever at which the tip locates. 44

Figure 4.11 An exhibition of tips with various shapes made by our process. The feasibility to different tip surface is confirmed. 45

Figure 4.12 SEM images of random shape obtained due to the bad quality of the original tip. 46

Figure 4.13 The SEM images of the same tip captured in (a) lateral side and (b) backside. It is clearly seen that the dimension decreases significantly in one direction but remains the same in the other direction. 46

Figure 4.14 Screenshots of a fabricated tip scanning high-density pillar arrays. (a) The tip scans in a random direction but hard to reach the bottom at most regions, (b) the tip scans in a direction perpendicular to the previous one and reaches the bottom in all regions. 47

Figure 5.1 Contrast curves for the PMMA-ZEP mixture resist, as well as for pure PMMA and ZEP resist. The resists were exposed at 20 keV and developed in amyl acetate for 1 min. The ratios in the graph were volume ratios of PMMA: ZEP. 52

Figure 5.2 Line array resist structures after electron-beam exposure and development using amyl acetate for 1 min. (a-b) 200 nm array periodicity. (c-f) 500 nm array periodicity. The top layer is PMMA, and the bottom layer has a PMMA: ZEP volume ratio of 2:1, 1:1, 1:2 and 0:1 (pure ZEP). The lines collapsed or detached for (e-f) because of capillary force when the undercut was too large or even merged together. 55

Figure 5.3 Cr line arrays with 100 nm thickness and 500-nm-array periodicity fabricated by lift-off using the bi-layer resist, consisting of top PMMA layer and bottom PMMA: ZEP mixture with the volume ratio of 2:1 (a), 1:1 (b), 1:2 (c), and 0:1 (pure ZEP) (d). 55

List of Tables

Table 2.1 The comparison of thermal evaporation and electron-beam evaporation in various aspects. 8

Chapter 1 Introduction

This chapter gives a brief introduction to nanofabrication.

1.1 What is nanotechnology?

At its early stage, nanotechnology was vaguely described as the manipulation of matters on an atomic, molecular and supramolecular scale. A more generalized description was then established by National Nanotechnology Initiative, which defines nanotechnology as the technology dealing with matters that reside in the scale from 1 to 100 nanometers (nm) in at least one dimension.[1] Figure 1.1 shows the comparison of the sizes of different objectives in nanometers. This definition was broadly accepted and became a research category that includes various types of researches dealing with specific properties of the matters that fall in this scale. Nowadays, nanotechnology includes fields as diverse as surface science, organic chemistry, molecular biology, semiconductor physics, microfabrication, molecular engineering, etc. [2] The applications are therefore equally diverse, ranging from nanoscale device fabrication to developing new materials.

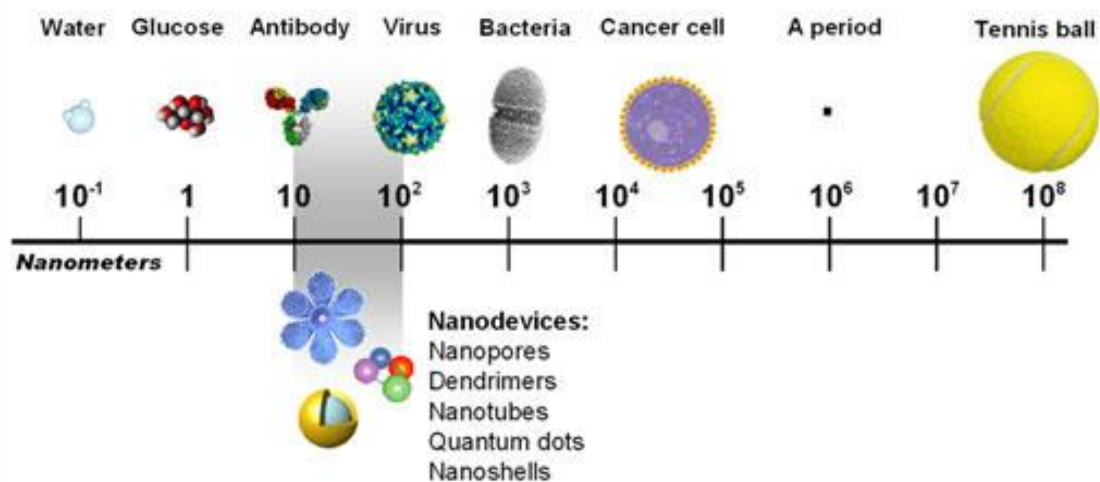

Figure 1.1 Sizes of different objectives in nanometers (Picture courtesy to the National Cancer Institute).[3]

1.2 Overview of Nanofabrication

Nanofabrication is the technology that is capable of constructing desired structures in nanoscale. It plays a fundamental but critical role to nearly every aspect of nanotechnology including nanomaterials research and nano device development. The last decade witnessed the prosperous development of manifold techniques that fulfill the demands of nanotechnology and nanofabrication. [4-7] Large scale, commercial implementation of nanofabrication accomplished unprecedented development in information technologies, for instance, microprocessors and ultra-high-density memory chips, etc. In order to make all these applications come real, nanofabrication approaches with ultimate precision and the complete control of the processed materials are required. In general, the nanofabrication approaches can be divided into two categories: "top-down" and "bottom-up". Figure 1.2 shows the schematic of both the top-down (a) and the bottom-up (b) approach.

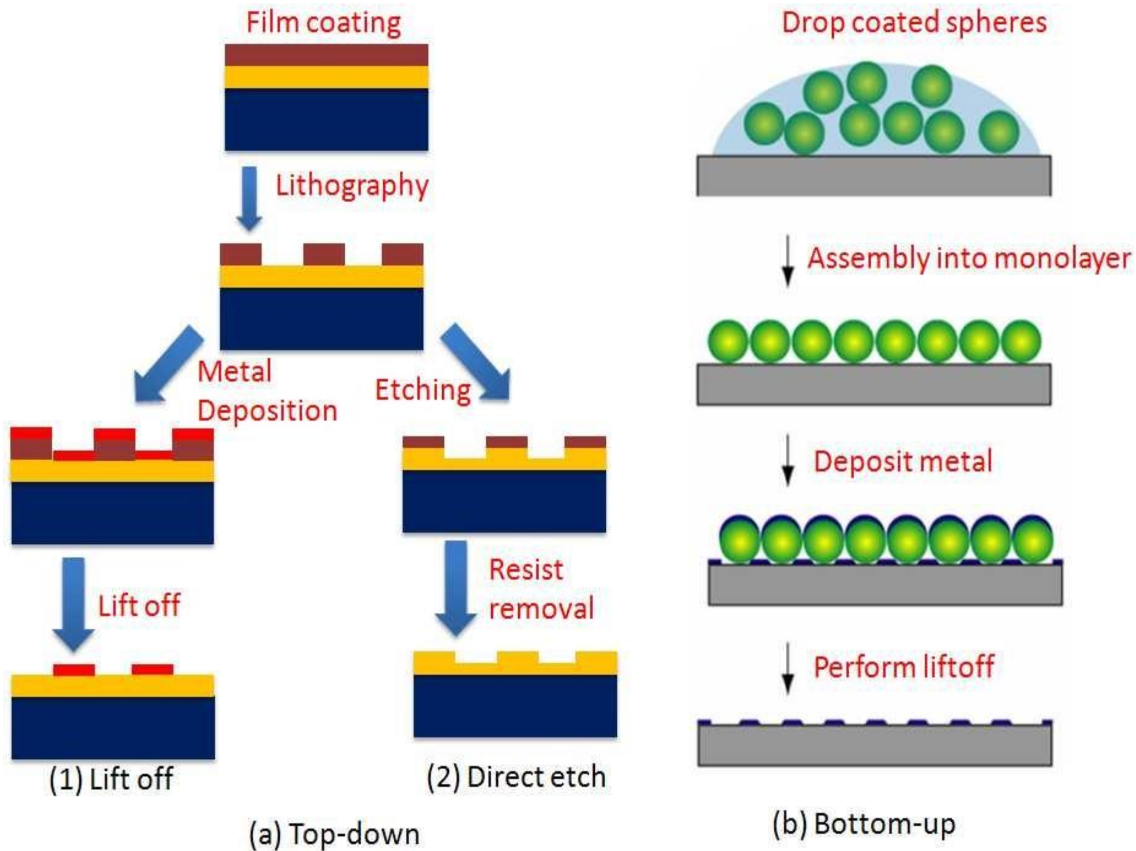

Figure 1.2 The schematic of the (a) top-down and the (b) bottom-up approach. In the top-down approach, the resist is first patterned by lithography, and then (1) the pattern is transferred by deposition followed by liftoff, or (2) the pattern is transferred by direct etching. In the bottom-up approach, the pattern is usually acquired by self-assembly and then transferred onto substrates by liftoff.

In general, the top-down approach creates nano structures starting from larger dimensions and then reduces them to the desired scale. The techniques that often involved are lithography, thin-film deposition and etching.

Various methods of lithography have been implemented in the top-down approach. As the predecessor of all other lithography methods, photolithography (or optical lithography) was first introduced to the integrated circuits (IC) industry in 1960's.[4] Conventional photolithography employs light to expose the photoresist, an organic light-sensitive material that can be coated onto the substrate, through masks. There are two types of photoresists. If a positive photoresist is illuminated, the exposed areas will be highly soluble in the developing solutions and therefore, these areas can be removed. In contrast, the areas in a negative photoresist is going to become insoluble in the developing solutions upon exposure. Hence these areas will remain as the required structures meanwhile the unexposed areas will be removed by the developing solutions.[4, 8] Conventional photolithography can only achieve a resolution around 1 μm. Several resolution enhancement techniques (RET) have been developed such as off-axis illumination (OAI), phase shift masks (PSM) which leads to the resolution down to sub-10 nm. Due to its low cost and large output, photolithography is always popular in industry. Unlike photolithography, electron-beam lithography does not need any masks and provides the ability of direct patterning, thus is also popular in IC manufacturing. In sum, lithography methods nowadays reside in one of two categories: serial or parallel. Parallel lithography techniques include photolithography, x-ray lithography (XRL), deep ultra-violet lithography (DUVL), extreme ultraviolet lithography (EUVL) and nanoimprint lithography (NIL). All of them can finish patterning in one run therefore feasible for massive production. Serial lithography techniques include electron beam lithography (EBL), ion beam lithography (IBL) and scanning probe lithography (SPL). [9] They don't need masks but take much longer time to pattern because they must expose the patterns one-by-one. Hence these lithography techniques are more suitable for R&D purpose or mask/mold fabrication.

Addition and subtraction of materials are both important in nanofabrication. Thin-film deposition is an additive method to introduce the materials needed for nanofabrication. There are two broad categories: physical deposition and chemical deposition. Physical deposition are techniques that materials are released from a source and deposited onto the samples without any chemical processes involved, for instance, by using mechanical, electromechanical or thermodynamic processes. The physical deposition can be further divided into two types: evaporation and sputtering. Evaporation will be introduced in the

next chapter. On the other side, chemical deposition implements volatile precursors to produce chemical changes on the surface of the samples and leaves deposited coatings there. Various types of chemical vapor depositions (CVD) are available nowadays such as metal-organic CVD, plasma-enhanced CVD, low-pressure CVD, etc.[8]

On contrary, the subtraction of the materials is obtained by etching techniques. Depending on if the liquid etchant is involved, etching techniques can be divided into two categories: wet and dry. Wet-etch employs liquid etchants to remove materials, which makes it simple and cheap but hard to control. Dry-etch, on the other hand, uses gas phase etchants in the plasma to etch out the undesired materials. More details of both etching techniques can be found in the next chapter.

Instead of starting from larger dimensions, bottom-up approaches start with building up molecular or atomic components into more complex nanoscale assemblies. Atoms, molecules or supramolecular elements can be driven by chemical reactions to spontaneously assemble into larger nanoscale structures.[10] Block co-polymer self-assembly, porous anodized aluminum oxide and nano-sphere lithography are the three most important self-assembly techniques that draw lots of interests. The bottom-up approaches having an apparent advantage of low cost and less waste of materials, however, are not suitable for lots of applications because they create almost only ordered or periodic structures. But bottom-up approaches are comparatively new, and therefore, they still have lots of potentials in the future. [11]

Chapter 2 Specific techniques for AFM probe fabrication

This chapter discusses the details of evaporation, reactive ion etching (RIE) and wet etch that are employed in batch fabrication of our direct positioning AFM tip. Important concepts and parameters in each technique are discussed.

2.1 Evaporation

As discussed in the previous chapter, evaporation is one of the physical vapor deposition techniques and it generally consists of two steps. First, the desired source material is heated above its melting points. Second, the evaporated material atoms travel to the substrate and condense on it to form the thin film covering the surface. Figure 2.1 shows the picture of a modern evaporation system. Due to its simplicity of operation, evaporation is extensively used in early IC industry.[1] Metals and metal compounds such as Chromium, Aluminum, Copper, Titanium Nitride are the materials that are most frequently deposited by evaporation.

Figure 2.1 The picture of a modern evaporator for R&D purpose. (Picture courtesy to the Intlvac Thin Film Corporation) [2]

Depending on the methods of generating the high temperature needed to release the source material, evaporation can be divided into two categories: thermal evaporation and electron-beam evaporation.

In thermal evaporation, heat is created by means of the electrical current passing through a filament or RF coils surrounding the graphite crucible that contains the source material. Figure 2.2 (a) illustrates the schematic of thermal evaporation. Because the heat created in this way is limited, the materials suitable for thermal evaporation is almost exclusive to those having evaporation temperature at 1600℃ or below. Furthermore, a significant drawback of thermal evaporation is that the filament or the crucible is heated as well as the source material. Such simultaneous heating will lead to high impurity in the deposited film.[3] Therefore, thermal evaporation is gradually replaced by electron-beam evaporation. However, thermal evaporation is the only choice for evaporation of organic materials.[4]

In electron-beam evaporation, the heat is produced by the high energy electron beam bombardment. The electron beam is generated by an electron gun and the emitted electrons are accelerated by an electrical potential as high as 10 kilovolts. The local temperature at the surface of the source material can reach 3000℃ and all the way up to 10000℃. If the electron gun is positioned below the crucible, the electron beam is often directed and bended by the applied magnetic field so that the electron beam trajectory can reach the surface of the source material. Figure 2.2 (b) shows the schematic of electron-beam evaporation. Since the electron bombardment is able to be focused on the sample, localized heating of the source material helps avoid heating of the crucible. Therefore, less contaminations from the crucible can be achieved. Table 2.1 shows comparison of thermal and electron-beam evaporation in several aspects.

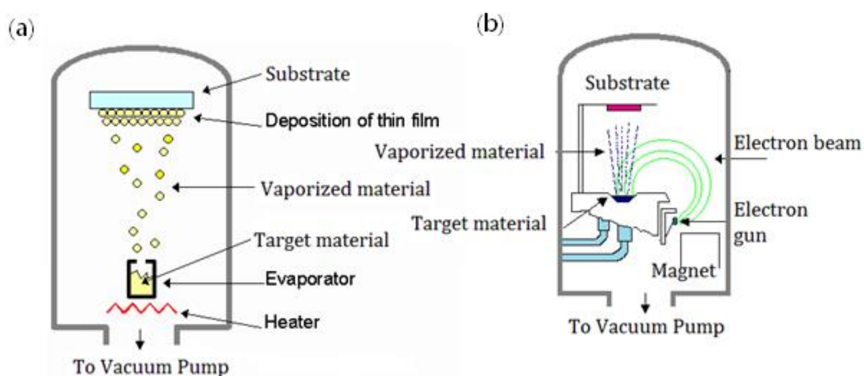

Figure 2.2 The schematic of (a) thermal evaporation and (b) electron-beam evaporation. (Courtesy to Hivatec Laboratory).[5]

Deposition Category	Material	Typical evaporant	Cost	Temperature Range	Impurity
Thermal	Metal, organic materials	Au, Ag, Al, Cu, Cr, Sn, Polystyrene…	Low	$\leq 1600°C$	High
Electron-beam	Metal and dielectrics	Everything above plus: Ni, Pt, W, Ta…	High	$\geq 3000°C$	Low

Table 2.1 The comparison of thermal evaporation and electron-beam evaporation in various aspects.

There are several critical parameters in the evaporation process. First, either thermal or electron-beam evaporation must be carried out in the high vacuum level. The pressure in the operating chamber determines a very important film-deposition parameter called the mean free path. The mean free path of a gas molecule amounts to the average distance the molecule travels before it collides with another molecule. Apparently, less collisions of source material molecules before reaching the target substrate is desired, which means the larger the mean free path the better the deposition quality. The mean free path λ satisfies the relation below:

$$\lambda = \frac{kT}{\sqrt{2}\pi p d^2} \tag{2.1}$$

where *k* is the Boltzmann constant, *d* is the diameter of the gas molecule, *T* is the temperature in the chamber and *p* is the pressure in the chamber. Clearly, when the temperature and the diameter of the gas molecules are known, mean free path is inversely proportional to the pressure in the chamber. Hence the high vacuum level is required to keep the mean free path large. Normally, the pressure demanded is near or below 10^{-4} Pa. For instance, a 4-Å molecule has a mean free path around 60 meters at this pressure whereas the distance between the target substrate and the source material is often smaller than 1 meter.[3] The second important parameter is the deposition rate. Naturally, high deposition rates are always preferable because it improves the productivity. Furthermore, a high deposition rate also improves the purity of the thin film deposited at a given vacuum pressure since it minimizes the rate of background gaseous impurity inclusion. Meanwhile, no unknown effects of high deposition rate on the film structure have been found.[6] Although the deposition rate is dependent of specific geometry of the working chamber,

the film quality is generally related to the energy of the injected beam. The higher the energy of the beam, the higher the temperature of the source material and the greater the kinetic energy of the molecules at its surface. Therefore, one can increase the deposition rate simply by raising up the energy of the electron beam. The common method of monitoring the deposition rate implements the quartz crystal, which is covered by the evaporation material during the deposition. The resonant frequency of the crystal shifts in proportion to the thickness of the deposited film so that the deposition rate can be calculated.[3]

Last but not least, it is critical to monitor the thickness of the deposited film. Unlike the deposition rate, the quartz crystal mentioned in the last paragraph explicitly shows the thickness of the deposited film. However, the quartz crystal and the target substrate are often not placed together, which means that there will be a slight variance between the thickness on the substrate and the thickness on the quartz crystal. It is therefore important to monitor the real thickness instead of reading the direct measurement returned by the quartz crystal. The details of monitoring the real thickness will be discussed in Chapter 4.

Also, there are some inevitable issues for the evaporation. The first is the uniformity across the deposited film. For the substrate with a flat surface, the distance from the center of the substrate to the source and the distance from the edge of the substrate to the source are different. Therefore, the deposition rate at the center and the edge of the substrate are also different. If we define the uniformity σ:

$$\sigma = \frac{R_1 - R_2}{R_1} \tag{2.2}$$

where R_1 and R_2 are the deposition rate at the center and the edge of the substrate respectively, then the distance between the source and the substrate, namely *r*, has to satisfies the relation:

$$r > \frac{W}{\sqrt{2\sigma}} \tag{2.3}$$

where *W* is twice the distance between the center and the edge of the substrate. In practice, *r* is around 40 centimeters.

Another issue of the evaporation is the shadowing. Because the large mean free path of the gaseous source molecules at the low pressure, evaporation tends to be highly directional. Figure 2.3 illustrates the shadowing problem that occurs with closely spaced features. In the fully shadowed region, little deposition can appear. In chapter 4, we will show that the shadowing can be exploited to create the structures we need. But in most cases, planetary substrate holders that continuously rotate the wafer during the evaporation can be exploited to reduce this problem.

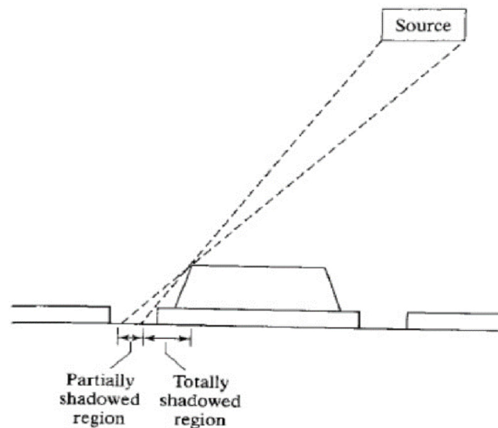

Figure 2.3 An example of the shadowing problem that may occur during the evaporation.[3]

In conclusion, as the oldest method of film deposition, evaporation has been gradually replaced by some other modern techniques like sputtering in industry. However, it is still powerful and popular in terms of R&D purpose. Its low cost, simplicity and versatility are still attractive to the AFM probe fabrication.

2.2 Etching

Etching serves as the subtracted process that selectively removes the thin film of unwanted region and results in desired patterns. There are three important parameters in the etching process. The first one is the etching rate. If etching is intended to make cavities or remove one entire layer of the multilayer system, the etching rate is then defined as the depth of cavities or the entire layer that is etched out per unit time. The second important parameter is the selectivity *S*, which is defined as the ratio of the etching rate between different materials. As mentioned above, the intention of etching is to remove the certain material at the certain region specifically. Therefore, etching has to be done without affecting other areas or other layers. This means that a high selectivity is normally preferred between materials. Figure 2.4 illustrates the difference of the etching results in terms of poor and high selectivity. The third critical parameter is the isotropy. If the etching process is proceeding in all direction equally, then such etching is

called isotropic etching. On the other hand, if etching is only significant in one specific direction, it is called anisotropic etching. Figure 2.5 shows the schematic of isotropic and anisotropic etching.

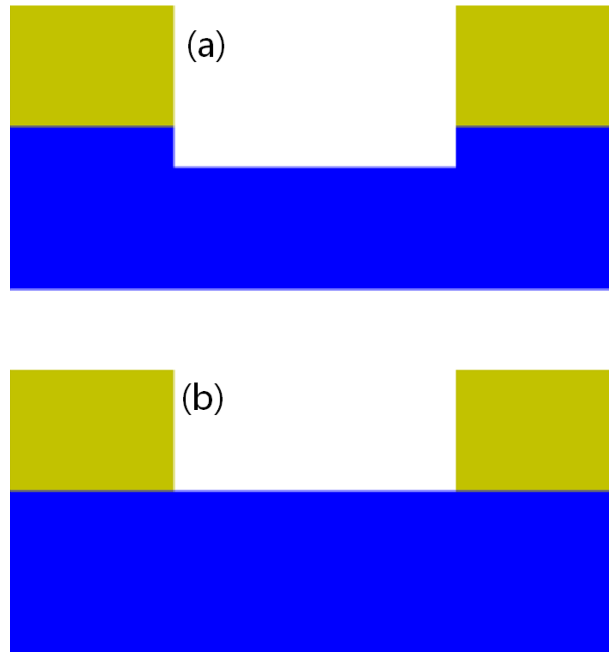

Figure 2.4 A graphical representation of (a) a poor selectivity causes the etchant to attack the bottom layer material while removing the top layer, (b) a high selectivity causes etch out the top layer without affecting the underlying layer.[7] (Courtesy to Smack.)

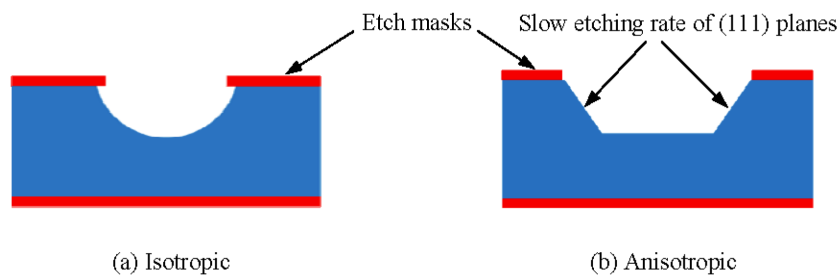

Figure 2.5 A schematic of (a) isotropic etching that has equal etching rate in all direction, and (b) anisotropic etching for which the etching rate is slower in <111> planes.[8]

Based on the type of the etchant, etching process can be generally divided into two categories: wet etch and dry etch. If the etchant are liquid chemicals, it can be defined as wet etch. Meanwhile dry etch normally implements gas phase etchant to remove the desired materials.

2.2.1 Wet etch

Wet etch is used extensively in nanofabrication processing. It is especially powerful for blanket etches of silicon (Si), oxide and metals, etc. Before 1970's, wet etch was almost the exclusive method in etching process when features were often larger than $3\mu m$. For small scale features, wet etch tends to make significant critical dimension loss. Therefore, today's IC industry only uses wet etch for noncritical feather sizes. Normally, wet etch is performed by immersing the wafers in the solution of the etchant or spraying etchants to the wafers.

The mechanisms for wet etch consists of three essential steps, as illustrated in Figure 2.6. Firstly, the reactants are transported by diffusion to the surface to be etched. Then, chemical reactions between reactants and the material that needs to be removed will occur at the reacting surface. Lastly, the reaction products from the surface are removed by diffusion. If the wafers are processed by immersion, mechanical agitation is always wanted to ensure good etch uniformity and a consistent etch rate. Nowadays spray etching are more popular in industry because it constantly supplies fresh etchant to the reaction surface. Hence the etch rate can be significantly increased in spray etching.

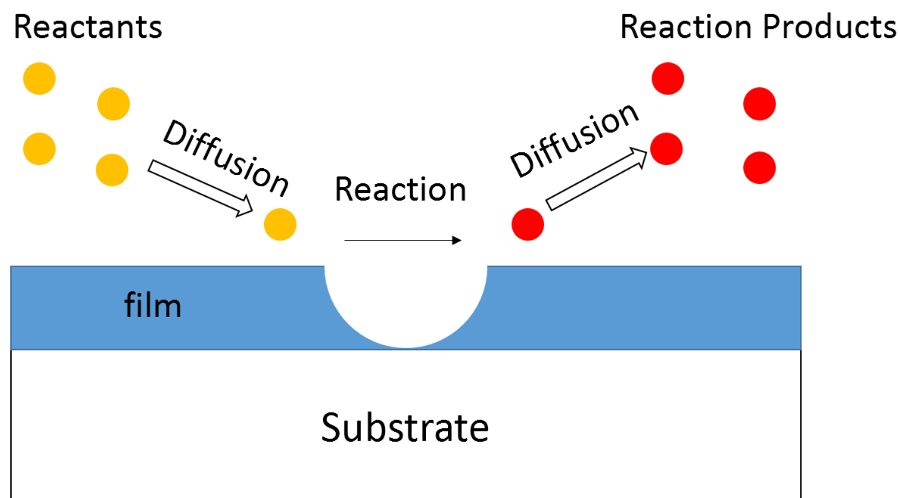

Figure 2.6 An illustration of wet etch process. Reactants first diffuse to the surface of the film to be etched. Then reactions are going to take place. Lastly, the products of the reaction diffuse away by the liquid flow in the solution of the etchant.

Although wet etch is isotropic in most cases, it is still able to achieve anisotropic profiles. Different specialized etchants can be used to certain surfaces in order to etch it in an anisotropic way because these

etchants remove crystalline materials at very different rates depending upon which crystal plane is exposed. A very famous example is using alkaline liquid solvents, such as potassium hydroxide (KOH) or tetramethylammonium hydroxide (TMAH) to etch silicon wafer. All of them are hot aqueous caustics. For a silicon lattice, there are three noteworthy crystal planes noted as <111>, <100>, <110> by Miller index. Figure 2.7 gives a graphical representation of these planes. For a silicon lattice, the <111>-plane has more available bonds per unit area than the other two planes. Hence the etch rate is expected to be slower for the <111> plane.[9] For instance, a solution with 19 wt % KOH in deionized (DI) water at around 80℃ removes the <100> plane at a much higher rate than the <110> and <111> planes. To be more specific, the ratio of the etch rates for the <100>, <110> and <111> planes is 100:16:1 respectively.[9] And TMAH shows a selectivity of 37 between <100> and <111> planes in silicon. Anisotropic etching of <100>- oriented silicon through a patterned silicon dioxide mask creates precise V-shaped grooves and U-shaped grooves if the window in the mask is sufficiently large or if the etching time is comparatively short.[10] A visual representation is given in Figure 2.8. The sidewalls are <111>-oriented and have an angle to the surface of:

$$arctan\sqrt{2} = 54.7° \tag{2.4}$$

The width of the bottom of the U shape is given by:

$$W_b = W_0 - \sqrt{2}D \tag{2.5}$$

where W_0 is the width of the window in the mask and D is the depth of the etch.

The undercut δ, also called etching bias, is given by:

$$\delta = \frac{\sqrt{6}D}{S} = \frac{\sqrt{6}R_{100}T}{R_{100}/R_{111}} = \sqrt{6}R_{111}T \tag{2.6}$$

where D is the etch depth, S is selectivity between <100> and <111> plane, R_{111} is the etch rate in <111> plane, R_{100} is the etch rate in <100> plane and T is the etch time.

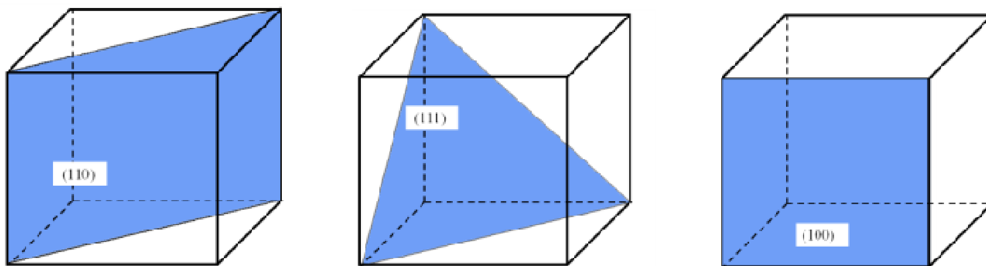

Figure 2.7 A graphical illustration of three major planes in a cubic unit silicon.[8]

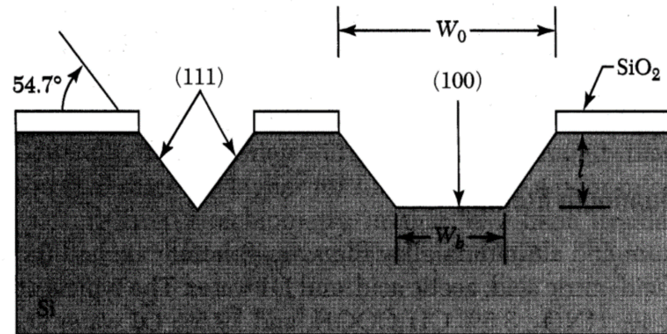

Figure 2.8 An illustration of a V-shaped groove and a U-shaped groove.

On the other hand, acids are always able to wet etch metals or alloys. One typical etchant for Aluminum is the solution of 80% phosphoric acid, 5% nitric acid, 5% acetic acid and 10% DI water (PAN) at 30°C- 80°C.[11] Nitric acid first oxidizes aluminum with the assistance of acetic acid and then phosphoric acid dissolves the oxidized aluminum. Generally, wet etch of metal and insulating films is achieved in a similar way. Chemicals, often acids, first convert metals or insulating materials into their soluble salts or complexes and then dissolve these materials in their bulk form. Figure 2.9 shows a table of various materials and their wet etchants. Etch rates are always determined by the concentration of the etchant, temperature, agitation and impurities in the materials to be etched.

Material to be etched	Wet etchants
Aluminium (Al)	80% phosphoric acid (H_3PO_4) + 5% acetic acid + 5% nitric acid (HNO_3) + 10% water (H_2O) at 35–45 °C[4]
Indium tin oxide [ITO] (In_2O_3:SnO_2)	Hydrochloric acid (HCl) + nitric acid (HNO_3) + water (H_2O) (1:0.1:1) at 40 °C[6]
Chromium (Cr)	• "Chrome etch": ceric ammonium nitrate ($(NH_4)_2Ce(NO_3)_6$) + nitric acid (HNO_3)[7] • Hydrochloric acid (HCl)[7]
Gallium Arsenide (GaAs)	• Citric Acid diluted ($C_6H_8O_7$: H_2O, 1 : 1) + Hydrogen Peroxide (H_2O_2)+ Water (H_2O)
Gold (Au)	Aqua regia, Iodine and Potassium Iodide solution
Molybdenum (Mo)	
Organic residues and photoresist	Piranha etch: sulfuric acid (H_2SO_4) + hydrogen peroxide (H_2O_2)
Platinum (Pt)	Aqua regia
Silicon (Si)	• Nitric acid (HNO_3) + hydrofluoric acid (HF)[4] • Potassium hydroxide (KOH) • Ethylenediamine pyrocatechol (EDP) • Tetramethylammonium hydroxide (TMAH)
Silicon dioxide (SiO_2)	• Hydrofluoric acid (HF)[4] • Buffered oxide etch [BOE]: ammonium fluoride (NH_4F) and hydrofluoric acid (HF)[4]
Silicon nitride (Si_3N_4)	• 85% Phosphoric acid (H_3PO_4) at 180 °C[4] (Requires SiO_2 etch mask)
Tantalum (Ta)	
Titanium (Ti)	Hydrofluoric acid (HF)[4]
Titanium nitride (TiN)	• Nitric acid (HNO_3) + hydrofluoric acid (HF) • SC1 • Buffered HF (bHF)
Tungsten (W)	• Nitric acid (HNO_3) + hydrofluoric acid (HF) • Hydrogen Peroxide (H_2O_2)

Figure 2.9 A table of wet etchants for some common nanofabrication materials. (Contents courtesy to Wikipedia) [12]

2.2.2 Dry etch

Modern VLSI process often avoids wet etch because the etch rate is so sensitive to the ambient parameters like temperature and humidity. Therefore, the process is hard to be precisely controlled. Besides, most of the layer materials in nanofabrication, like silicon dioxide and silicon nitride, are amorphous or polycrystalline films, which generally leads to isotropic etch results. In order to solve these problems, dry etch was introduced into nanofabrication in late 1970's. Dry etch can also be referred as plasma etching because most dry etch techniques are operated with the assistance of the plasma.

Plasma is a fully or partially ionized gas composed of nearly equal numbers of positive and negative charges and another number of neutral molecules. It is produced by providing an electric field with sufficient magnitude to the gas, resulting in gas molecules to break down and become ionized. Mostly, the gas molecules employed in a plasma are noble gas like argon and halogens, etc. If the electric field is

provided by a direct current (DC) power input, it is DC plasma. Otherwise, it is call radiofrequency (RF) plasma. Figure 2.10 illustrates the structure in a DC plasma system. Once ionized, the resultant positive ions are accelerated towards the cathode and if it's covered by the wafers or other materials of interest, ion bombardment will appear on them. On impact, some secondary electrons will be ejected and get repelled from the cathode, causing an increased density of less mobile positive ions. Therefore, there will be a dark region appearing close to the cathode. At low pressures, the mean free path of electrons increase, leading to an increase in the width of this dark region. As a result, the energy with which ion strike the wafers is increased as well. However, if the material placed on the cathode is insulating materials, undesired positive charges will build up on the cathode. Hence, an alternating electric field acquired by RF input is necessary to replace DC input to avoid charge build-up for insulating materials. Furthermore, oscillating electrons following the switching of the anode and cathode are more efficient to ionize the gas.

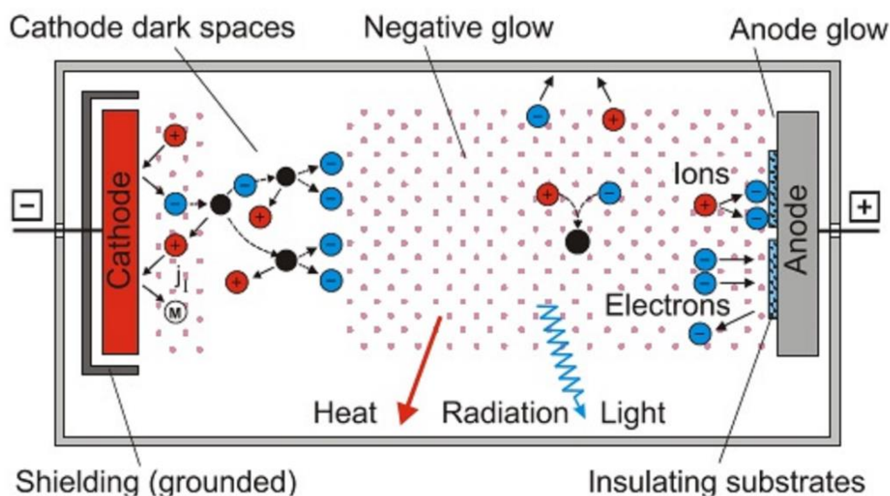

Figure 2.10 A schematic of the structure in a plasma. (Courtesy to Henrik Obst)[13]

If there are no chemical reactants added to the plasma, the dry etch can be achieved in a pure physical manner and it's called sputtering etching. Ionic species in the plasma are accelerated towards the electrode where the wafer to be etched lies. Then they strike the wafer surface, knock off the material to be etched. Because the ionic species are accelerated by the self-bias of the plasma which is perpendicular to the wafer surface, these ionic species will also mostly strike the wafer surface perpendicularly in low pressure regime. Consequently, sputtering etching is highly directional. Meanwhile, the ion bombardments take place uniformly across the wafer, and selectivity is thus very poor for sputtering etching.

Etching relying only on ion bombardment is not efficient and very time-consuming. In order to improve the etch rate, chemical reactants are introduced into the plasma. The etching process then becomes chemical etch assisted by physical ion bombardment. A very popular and powerful implementation of such etch technique is Reactive Ion Etch (RIE). The ionic species in the plasma result in high directionality, meanwhile the chemical reactive species (free radicals) lead to high etch selectivity. Control of ratio of ionic/reactive components in the plasma can modulate the etch rate and the etch profile achieved by RIE.[14] The mechanism of RIE can be divided into four steps as depicts in Figure 2.11. First, reactive species, both neutral radicals and ions are generated in the plasma. Then these reactive species transport to the target wafer and get adsorbed on the surface of the wafer to be etched. Reactions between the reactive species and the material to be etched take place at the wafer surface subsequently and create some byproducts. Lastly, byproducts desorb from the wafer surface, hence the etched structures appear.

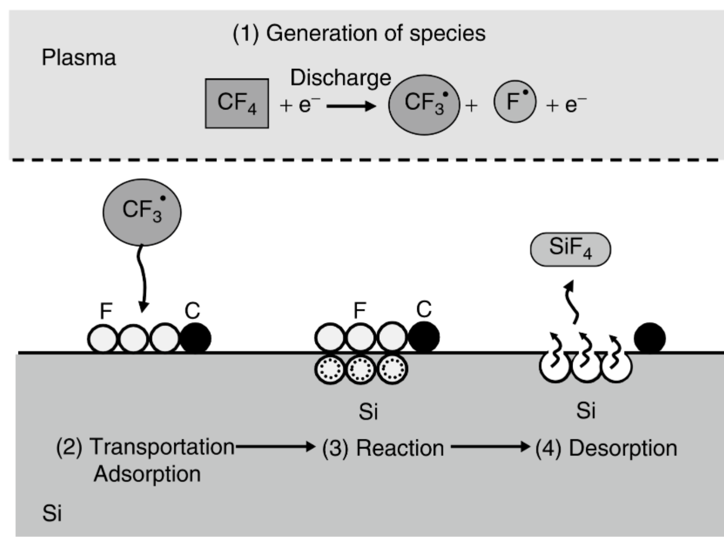

Figure 2.11 Reaction steps of RIE for the case of Si etching by using CF_4.[15,16]

Due to their low density, the ions don't contribute too much to the etch. So isotropic etching can still exist even with directional ion bombardments. In fact, the function of the ions is to help the chemical reactions in RIE. Ion bombardments enhance one of the following steps during chemical etch: surface adsorptions, etching reactions (by physically damaging the chemical bonds of the material to be etched), byproducts removal and removal of un-reacted etchants. Figure 2.12 compares the etch rates for sole chemical dry etch, sole physical dry etch and chemical etch with assistance of ions. It clearly proves that ion-assisted chemical etch is much more efficient.

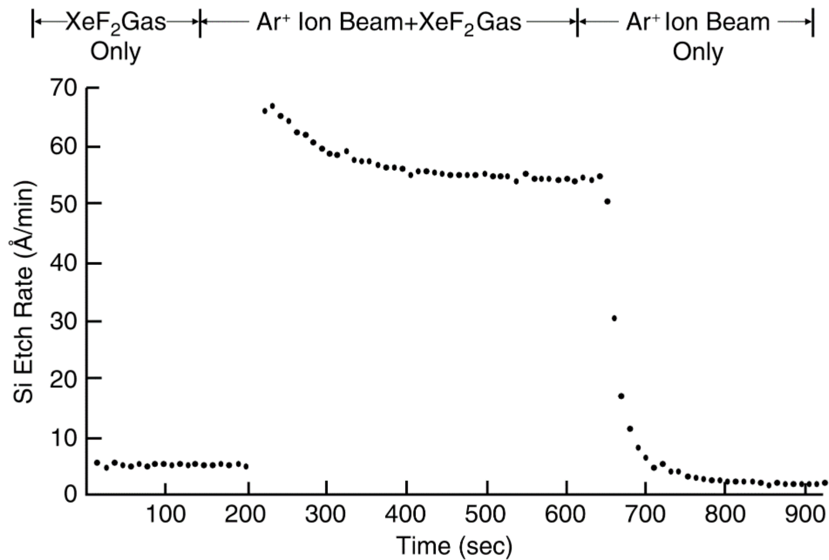

Figure 2.12 The graph compares the achievable etch rated by XeF_2 gas only, Argon ion plasma only and the combination of them. The combination of chemical and physical etch, namely ion-assisted chemical etch significantly improves the efficiency of the etching.[17]

Anisotropy in RIE is actually achieved by two mechanisms. First, ion bombardments disrupt an un-reactive target wafer and cause damages such as dangling bonds and dislocations, making the wafer more reactive towards etchant species. Improved chemical reactions on horizontal surface amount to high etch rates in vertical direction. Second, a protective layer (passivation layer) can be formed in RIE. When a mixture gas in which a gas for organic polymer formation is added to the plasma, monomers such as CF and CF_2 will be generated. These monomers will then adsorb to the wafer surface and start the polymerization. As a result, the entire surface of the wafer is going to be covered with polymers. When ion bombardments take place, ions coming in vertically remove the polymers on the horizontal surface meanwhile the polymers on the sidewall are hardly damaged. Therefore, almost no etching happens on the sidewall.

The effects of RIE vary among various combinations of the materials to be etched and the gas implemented. Generally, fluorine-based gases are extensively used to etch silicon. Mogab found a linear relation between the etch rate and fluorine-atom density showing that fluorine atoms are directly involved in the etching process.[18] A variety of additive gases such as hydrogen, nitrogen and oxygen can be introduced into RIE as well. Their function is to control the competition between the polymerization mentioned above and the etching so that different etching profiles are procured.[19] Nowadays the specific

choice of gas combinations, namely the recipe, is relying on empirical evidence obtained for a certain application. Particular recipe used for silicon etching is going to be discussed in Chapter 4.

Regular RIE employs low density plasma which leads to less amount of both ions and free radicals. Thus the etching rate is often slow. In order to improve it, high density plasma system was developed in recent years. In a RIE with high density plasma, ion flux and ion bombardment can be independently controlled while they are tightly coupled in regular RIE. High density plasma means much more efficient ionization and higher ion density in the system, which makes it possible to significantly increase the etch rate. Currently, high density plasma RIE represents an optimum compromise in high etch rates, good selectivity, good directionality, while with low ion energy and damage. High density plasma can be achieved by two techniques, either electron cyclotron resonance (ECR) or inductively coupled plasma (ICP). Both techniques take advantage of magnetic field to elongate the trajectory of electrons so that they have more chance to make collisions, and thus increase the ionization probability within the plasma.

Chapter 3 Introduction to Atomic Force Microscope Probe Fabrication

This chapter gives detailed introduction to AFM in terms of its history, principle of operation, fabrication method and AFM with carbon nanotube tip.

3.1 History

After scanning tunneling microscopy (STM) was first invented in 1981, the ability to image surfaces at atomic level was finally possible. For an STM, good resolution is considered to be 0.1 nm lateral resolution and 0.01 nm depth resolution.[1]

As the scanning tunneling microscopy became more and more useful and popular, its limitations emerged and drew scientists' attention. One of the main constraints of STM is the requirement of sample conductivity. Such limitation encouraged the invention of the new type of microscope, atomic force microscope, which could overcome this limitation. In 1986, Gerd Binnig, Calvin Quate and Christoph Gerber first proposed the atomic force microscope (experimental setup is shown in Figure 3.1)[2]. They replaced the wire of a tunneling probe from the STM with a lever made by carefully gluing a tiny diamond onto the end of a spring made of a thin strip of gold.[2] This was the cantilever of the first AFM. The new system extends the possibilities of imaging non-conductive samples. Binnig and his colleagues acquired preliminary results in air demonstrating a lateral resolution of 30 Å and a vertical resolution less than 1 Å.[2] Commercial products were first available in 1988 and the gold/diamond combined lever was soon replaced by much more reproducible cantilevers manufactured by silicon lithography.[3] Many developments were achieved and new modes of operation have been invented for the AFM since then.

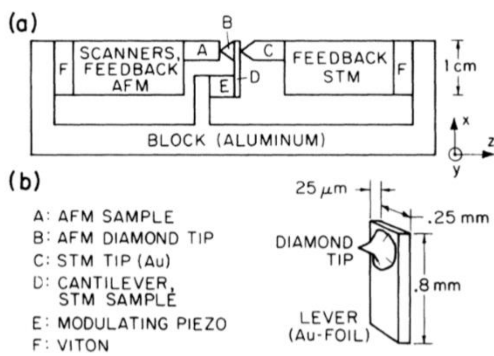

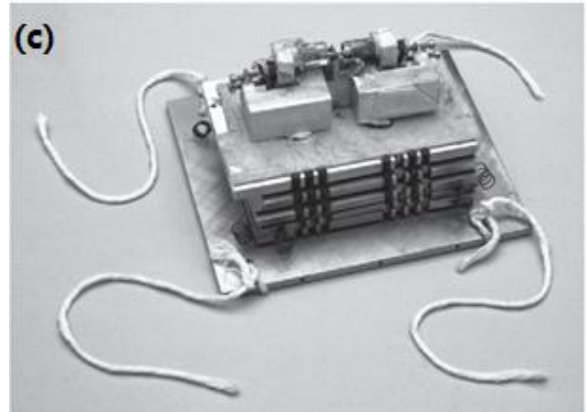

Figure 3.1 (a) Experimental setup of Binnig, Quate and Gerber's first AFM. (b) Its dimension. The STM and AFM piezoelectric drives are facing each other, sandwiching the diamond tip that is glued to the lever.[2] (c) The picture of the first AFM instrument (image copyright Science Museum London/SSPL).

3.2 Probe structures and characters

In an AFM, the entire probe includes a probing tip and a spring-like cantilever. The tip is always attached at one end of the cantilever. In order to handle the probe easily, a holder is attached on the other side of the cantilever. Figure 3.2 shows the schematic of a normal AFM probe and the typical dimensions of each part.

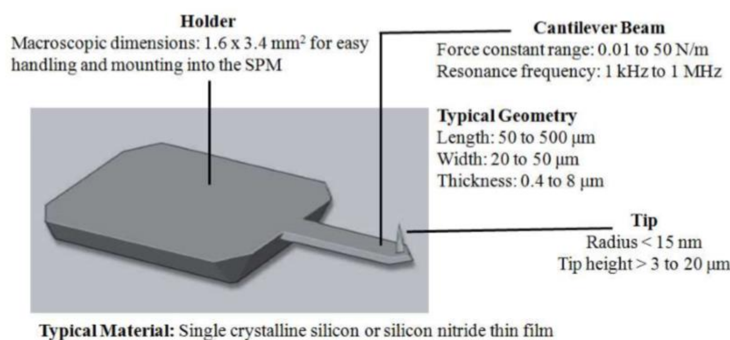

Figure 3.2 Schematic of a normal AFM probe and its dimensions. (Picture courtesy to Oliver Krause)[4]

A variety of probe materials have been employed but the most commonly used are microfabricated silicon (Si) or silicon nitride (Si_3N_4) cantilevers with integrated tips.[5] Meanwhile, abundant materials can also be coated on top of the probe to meet specific demands of application. For instance, metal films are

frequently coated onto probes made of undoped silicon or silicon nitride to improve its conductivity. Gold and aluminum are often coated on the back-side of the probe to enhance the reflection signal.

The most critical character of the tip is its radius. Nowadays tip radii of 5–50 nm are commonly available.[6] Normally the tip must be as sharp as possible but it also raises the problem of stability and flexibility when the radius decreases. The most important character of the cantilever is its spring constant and resonant frequency. Shorter and thicker cantilevers always result in larger spring constants and higher resonant frequencies.

3.3 Principle of Operation

As the successor of scanning tunneling microscope, the atomic force microscope is a combination of the principles of the scanning tunneling microscope and the stylus profilometer (SP). Instead of measuring the tunneling current between the sample and tip, the force in between is used to sense the proximity of the sample to the tip.

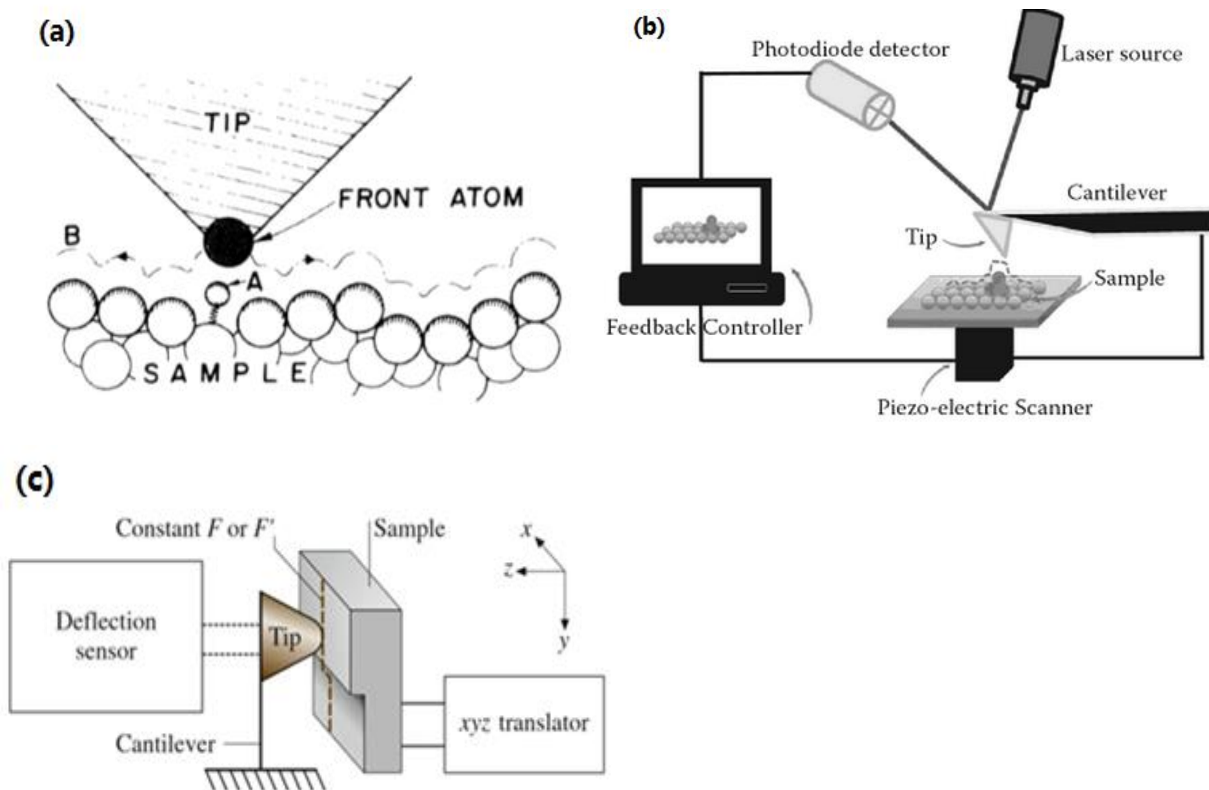

Figure 3.3 Description of the operation of the AFM. (a) Tip follows contour B to maintain constant force between tip and sample.[2] Brief schematic of AFM operations by measuring (b) cantilever deflection[5] (c) sample movement in z-direction.[6]

The sample topography is taken by maintaining same tip-sample distance and can be achieved in two ways. First, in order to maintain the same tip-sample distance, the cantilever is deflected while the sample remains unchanged in z-axis. The bending of the cantilever is usually monitored by the optical lever.[5] The optical lever employs a beam of laser to focus on the back of the cantilever and it will get reflected onto a photodetector (Figure 3.3 (b)). This system magnifies the normal bending of the cantilever greatly, and is sensitive to Angstrom-level movements.[5] Images are finally taken by digitizing the deflection of the cantilever. The second way requires a fixed cantilever deflection. The movement of the tip over the sample is controlled by a piezoelectric scanner, which can move precisely along x, y and z axes. The photodetector transmits signals through a feedback circuit into a xyz translator and then it tells the scanner the exact movement needed in z axis to maintain the tip-sample distance at the set value. Because the cantilever acts as a spring, this fixed cantilever deflection means a fixed tip-sample force is maintained.[7] The amount by which the scanner has to move in the z axis to maintain the cantilever deflection is taken to be equivalent to the sample topography.[7]

3.4 Fabrication methods

At the moment, massive production of AFM probes is implemented from whole silicon wafers. Figure 3.4 shows a picture of commercial wafers with probes on them.

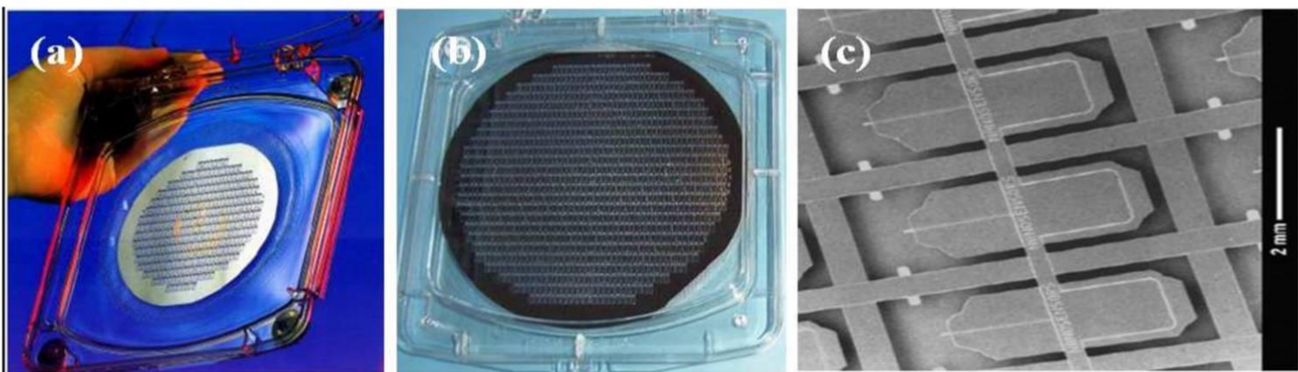

Figure 3.4 Image of commercial (a) 4-inch wafer with 380 probes, (b) 6-inch wafer with more than 1000 probes, (c) close look of tips on the wafer. (Picture courtesy to Oliver Krause)[4]

In the course of AFM probe development, two essential goals are pursued by most of the researchers. One goal is to find various materials that are applicable for AFM tips so that it is robust enough and the other goal is to achieve a tip apex as sharp as possible. These two goals then encouraged two mainstream methods of fabricating the probes. One method tries to define a silicon mold first with tip-shaped holes throughout the surface and fills them with desirable tip and cantilever materials thereafter. The probes can be achieved by removing the silicon mold by a wet silicon etchant. The other method applies the fabrication on the silicon wafer to get the structures directly. These two ideas, even not perfect, both have their advantages and show the great potential to meet the demands of different applications.

3.4.1 Indirect method

The so-called "indirect method" indicates that the entire process is not modified on the silicon wafers as usual. This method was first introduced in Albrecht's paper[3] in 1990. An inverse-pyramid-shaped cavity was first formed by wet etching onto a silicon substrate which only served as a mold. A layer of thin film was then deposited on the silicon and filled the cavity. Finally, the silicon substrate was etched back to detach the probe area. The tips fabricated by indirect method can be investigated by bonding another support layer (holder) to the silicon mold. Pyrex, for instance, is a popular choice for such support layer. The process flow of fabricating a normal nitride probe is described step by step in Figure 3.5[4].

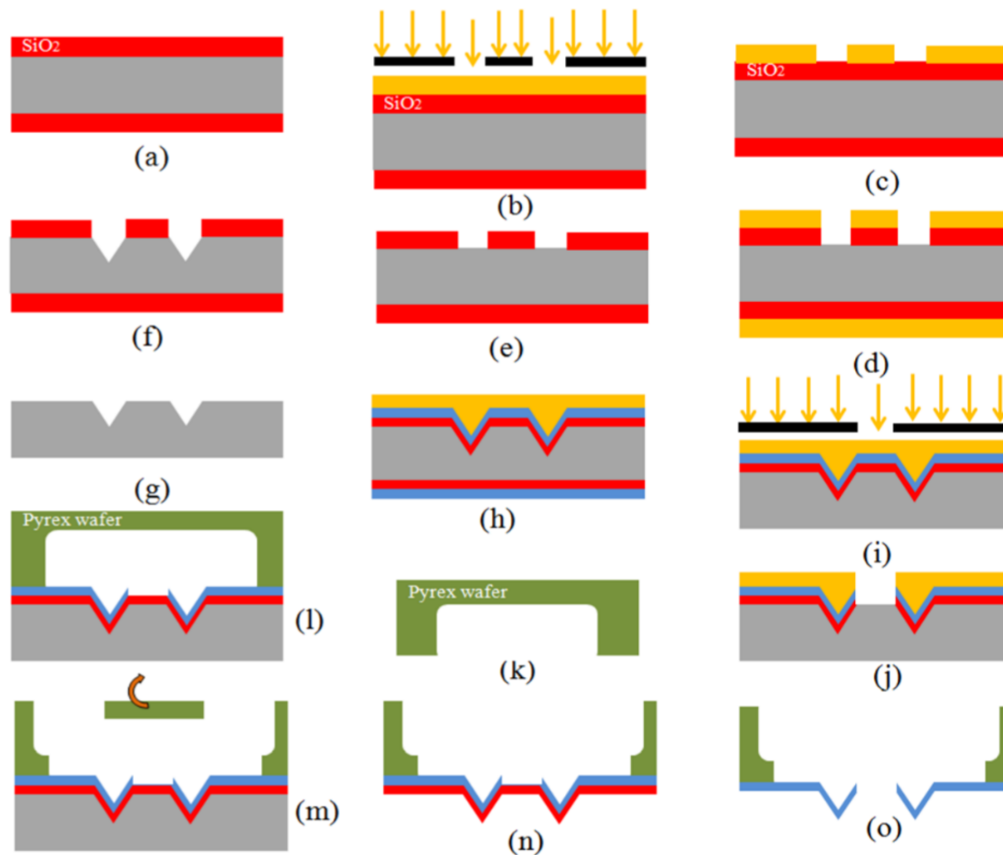

Figure 3.5 Fabrication steps of regular nitride probes. (a) thermal oxidation to coat oxide on both sides of silicon wafer (<100> orientation), (b) photolithography to expose resist, (c) resist development, (d) spin coating of protection resist on back side and etch oxide with BHF, (e) remove resist with acetone/isopropanol, (f) KOH wet etch to remove Si, (g) remove oxide with BHF, (h) grow oxide, deposit nitride, remove them on the backside, and spin-coat photoresist, (i) photolithography to expose the resist, (j) develop the resist and etch oxide then nitride, (k) dice Pyrex wafer (to be used as a handle), (l) anodic bonding the nitride and the Pyrex wafer, (m) dice and remove unnecessary portion of Pyrex, (n) KOH wet etch to remove Si, and (o) BHF etch to remove the oxide layer.[4]

One of the most critical advantage of this process is that it brings appreciable flexibility of selecting probe materials. Robust nitride tips that are frequently used in contact mode AFM are mostly produced by this method[3]. And options are not any more limited within semiconducting materials. Conducting materials like metals can be employed too. These metal probes are also necessary for the Scanning

Tunneling Microscope (STM). Therefore, AFM/STM combination are not impossible any longer. Another significant advantage is that the tips are all the time perfectly protected in the mold until the last process step. This helps reducing the risk of breaking the tip and thus improves the yield of the production. Nevertheless, indirect method was not as popular as direct method for a very long time. A fatal disadvantage of indirect probe fabrication is the difficulty of getting sharp or high aspect ratio tips. At the beginning, the cavity in the silicon mold was reported to be produced almost exclusively by KOH wet etching. It is acceptable for normal pyramid-shaped tips but they need to be further sharpened by oxidization after the fabrication. However, it is a disaster for high aspect ratio tips since KOH wet etching alone is not able to generate cavities that are deep enough.

A feasible solution was later investigated and introduced by A. Boisen and his colleagues[8]. In their experiments, a combination of wet and dry etching has been employed to create the mold for high aspect ratio tips. First, a 1 micrometer thermal oxide is grown on the low resistivity (100) silicon wafer, underneath a layer of 200nm silicon sputtered thereafter. This sputtered silicon acts like a masking layer instead of resist since resist is likely to harden too much and hence results in polymerization of the surface during oxide etching. Square and circular windows of different dimensions are defined on the silicon layer by photolithography and etched in SF_6/O_2 plasma. The patterns are then transferred to the oxide layer by using CHF_3/CF_4 plasma. Next, reactive ion etching (RIE) in SF_6/O_2 plasma will take place to create the deep cavity. A best oxygen percentage of 35, which create almost vertical side walls, was discovered by A. Boisen and their colleagues. The mold fabricated so far are very blunt thus a short KOH wet etching is supposed to take place and hit the bottom of the cavity. The rough bottom can become smooth and sharp in this way. The schematic in Figure 3.6 depicts the difference with and without the KOH wet etching.

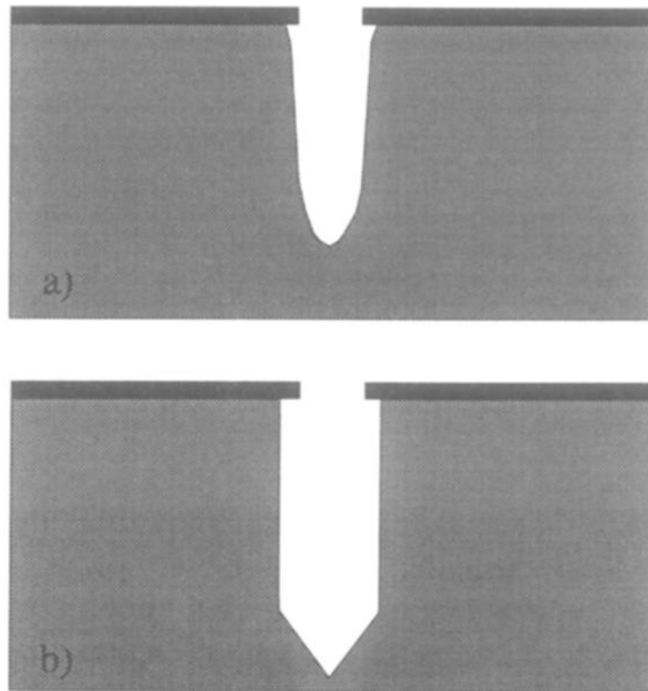

Figure 3.6 Schematic of the etching of mold by (a) RIE only and (b) a combination of RIE and KOH.[9]

In recent years, researches on graphene is booming. Due to its mechanical properties, graphene is an ideal material for AFM probes that is able to improve lifetime significantly. Therefore, researchers made efforts to employ graphene to fabricate the AFM probes. Martin Olmos and his group[9] showed that graphene can be grown uniformly over a seed copper layer which is on top of a silicon substrate. Graphene coated AFM probes are hence available. The brief process flow is illustrated in Figure 3.7. Tips they fabricated with the graphene layer were proven to acquire substantially improved lifetime. However, the group members also admitted that it is yet not fair to compare their probes with commercially available probes at the moment because of the unbearable large radii of their tips. Even though more efforts are needed to discover a way of stably producing sharp enough tips, the graphene probe still shows its promising future.

In conclusion, indirect method of fabricating AFM probes is desirable in many specific applications which require the versatility of probe materials. However, the tip sharpness is still a critical problem for such fabrication method even though there were some solutions that can improve it a bit. As the research on graphene boomed lately, it is predictable that more groups are going to make efforts to employ graphene as the AFM probe material. And indirect fabrication method seems to attractive to them.

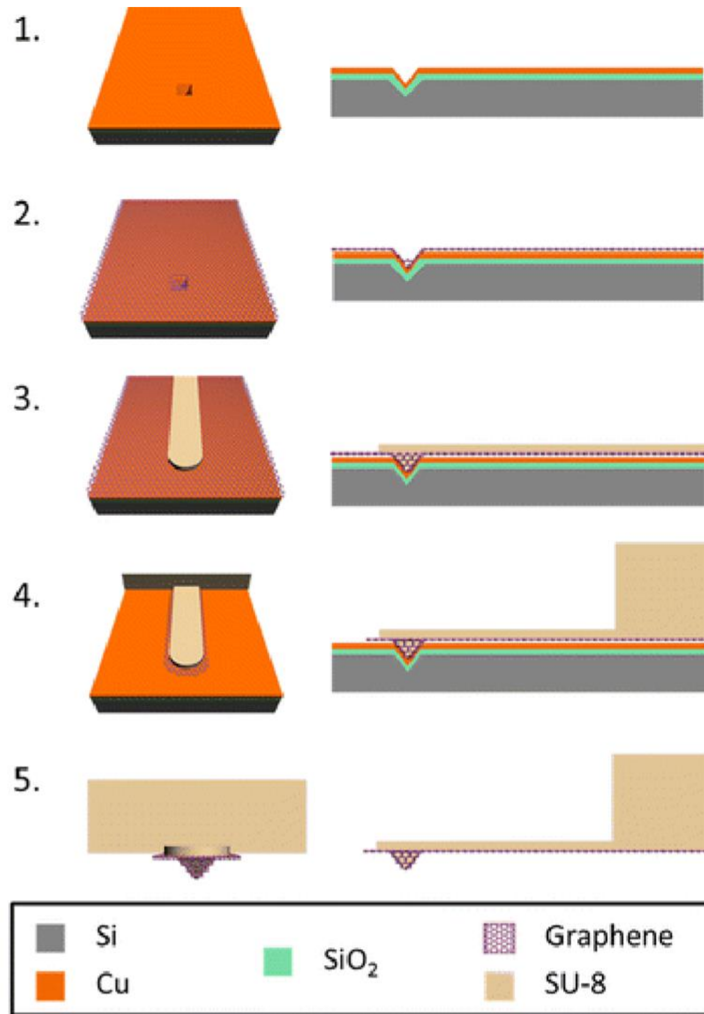

Figure 3.7 Fabrication process to make probe by molding scheme. (1) Prepare tip area by selectively etching of silicon with KOH solution. The pit and flat surfaces were grown with thermal silicon dioxide and finally coated with copper. (2) Grow a continuous layer of graphene on copper film by CVD method. (3) Coat a thin SU-8 resist to fill the tip mold; and expose and develop to define the cantilever. (4) Argon dry etch to remove the graphene elsewhere where there was no SU-8 film. Later, process a second and thick SU-8 to pattern the probe body. (5) After removal of silicon dioxide with HF solution, silicon with KOH and Cu with wet etchant, probe was released with graphene layer.[10]

3.4.2 Direct method

Instead of seeking the versatility of AFM probe materials, more groups of researchers were making efforts to improve the sharpness of AFM tips. And direct fabrication was proven to be more desirable to

this goal. Unlike indirect method, the entire process is implemented directly on the tip material. A layer of mask, photoresist for instance, will be first deposited on the front side of the silicon wafer <100>. After exposure and development, desirable areas on the entire mask are going to survive. Then the wafer will undergo reactive ion etching (RIE) or anisotropic wet etching to release the pillar that become the tip at last. An undercut of the mask is necessary next to get the tip apex. This undercut can be achieved from either KOH wet etching or isotropic RIE process using SF_6. Finally, the cantilever and holder are released by backside wet etch. A typical fabrication applying above process is explained in Figure 3.8.

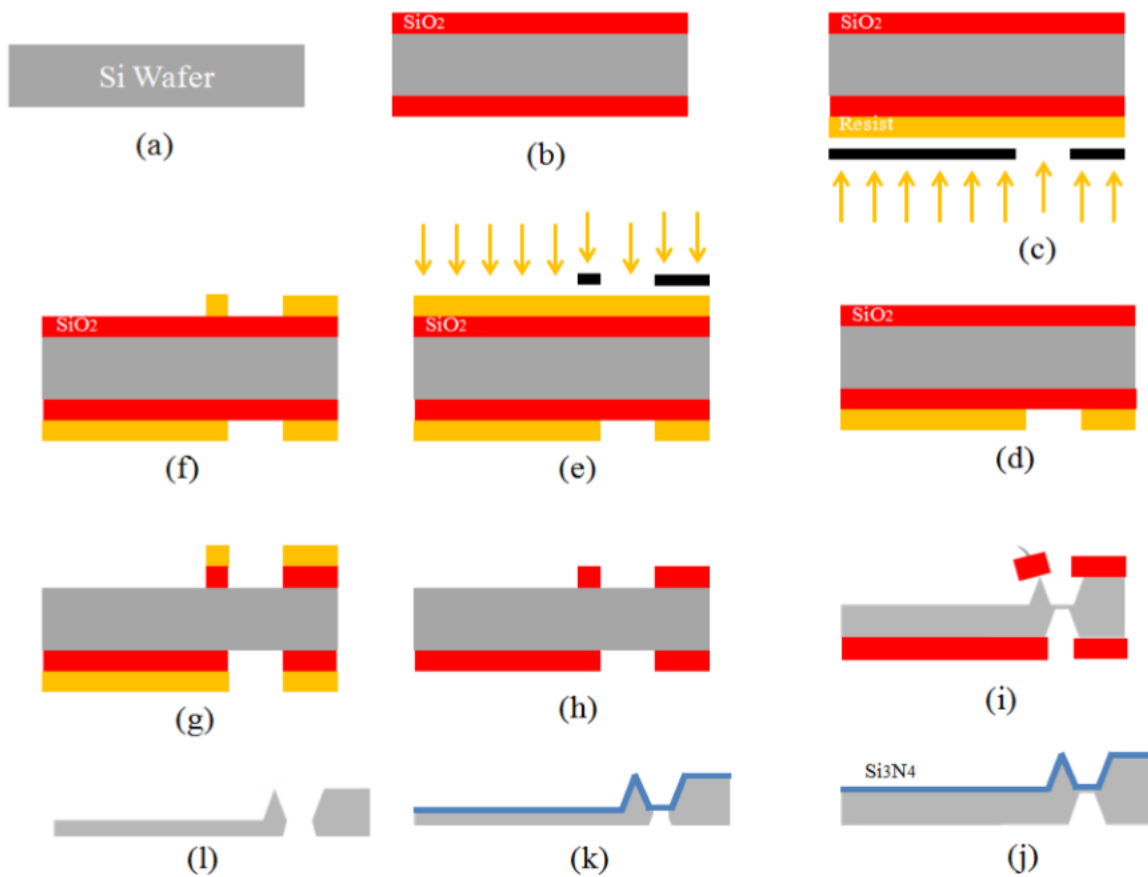

Figure 3.8 Fabrication steps of regular silicon probe. (a) Start with Si wafer, (b) next, coat SiO2 on both sides of silicon wafer (<100> orientation), (c) then, coat photoresist on back side of wafer and photolithography (exposure of the photoresist through a chromium/quartz mask) to define the cantilever back shape, (d) next, develop the exposed photoresist, (e) deposit photoresist in front side of the sample and photolithography to shape the cantilever top side, (f) development of the exposed photo resist, (g) isotropic wet etch to remove the silicon dioxide, (h) next, dissolve the photo resist, (i) anisotropic wet etch

with KOH to remove silicon. The formation of the tip is finished when the "oxide shield" falls off, (j) isotropic wet etch to remove silicon dioxide and then deposit the silicon nitride layer to protect the tip side of the probe, (k) next, anisotropic KOH wet etch to remove silicon from back side. The thickness of the cantilever is determined during this step, (l) finally, isotropic wet etch to remove the silicon nitride.[4]

A great advantage of direct method is its simplicity and low cost. Compared with indirect method, it is more straightforward and cheap chemicals are able to replace expensive machines like RIE during the entire process. But the most critical advantage of direct method which make it much more popular is that high-aspect-ratio tips are much sharper than those fabricated by indirect method. The deposition that is needed in indirect method has so many limits dealing with high aspect ratio structures. Thus the sharpness is very hard to transfer from the mold to the tip. On the opposite, the high-aspect-ratio structure can be achieved by deep silicon etching while tip is etched by KOH in direct fabrication. Two steps will not interrupt each other which easily keeps both sharpness and high aspect ratio.

Even though direct fabrication is very mature now, it still has some restrictions. First, direct fabrication is almost performed on silicon exclusively. The lack of material options results in tips to be less robust. Second, undercut carried out by wet etch is not a process that can be well controlled. The undercutting of the masks is never able to be uniform on a wafer scale thus the yield is always constrained. Third, the mask is going to fall down once the tip apex underneath is not large enough anymore to support it. And lack of mask leads to termination of undercutting at once. Thus further sharpening is always necessary after direct fabrication of probes.

3.4.3 Sharpening of the tips

The most broadly used technique for sharpening now is the thermal oxidation. This method was first reported by Marcus and his colleagues in their paper[10]. They observed that high stress can be an obstacle during the thermal oxidation process. The higher the stress, the lower the oxidation rate. And high stress always occurs at the place which has small curvature of radius. As a result, the oxidation is much slower close to the tip apex whose curvature of radius is very small. Thus by repeatedly growing oxide film on the tip and etching them away with HF, the probe tip can be sharpened. Marcus's group demonstrated their radii of curvature at the tip apex can be smaller than 1nm. The only barrier for oxidation

is that very high working temperatures are necessary (900-950℃). Figure 3.9 gives a more visual view of oxidation sharpening.

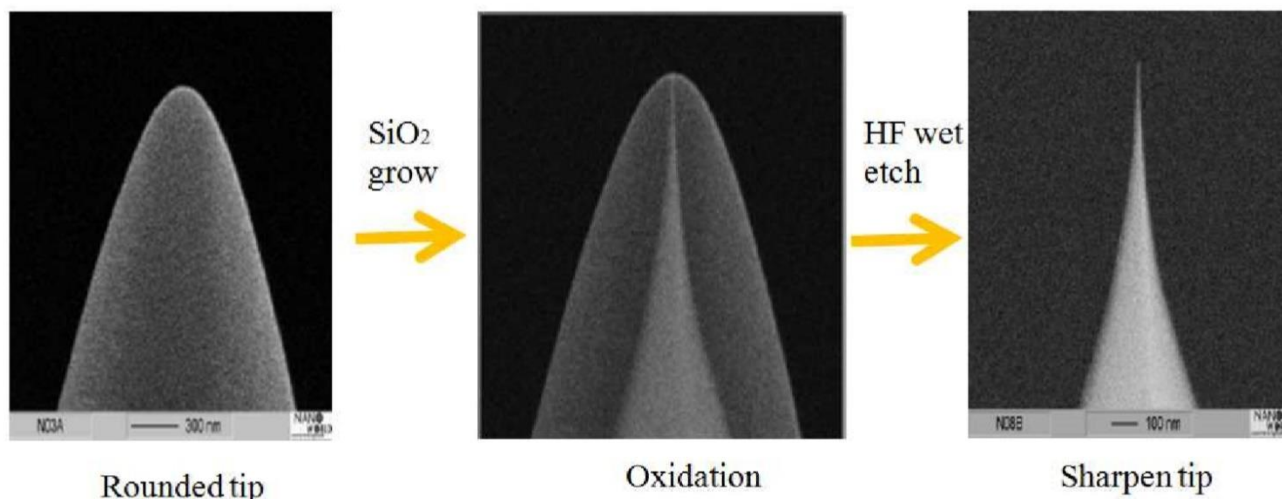

Figure 3.9 Oxidation sharpening process (Courtesy to Nanosensor).[11]

In conclusion, the direct fabrication is a popular method for the commercial product now. It is straightforward and low cost. And it works well especially for high aspect ratio tips. However, even though the direct method is very mature now, it is not perfect. The tip shape is almost exclusively created by KOH wet etch. But wet etch is not as uniform and reproducible as dry etch. Therefore, further researches are focusing on finding an alternative solution that can replace KOH wet etch perfectly and various ways to sharpen the tip.

3.5 Future of the AFM probe --- Carbon Nanotube Tips

Carbon nanotube (CNT) is a natural material for AFM tips because it has several exceptional mechanical properties that are perfect for tips. First, carbon nanotubes consist of a honeycomb sp^2 hybridized carbon network that is rolled up into a seamless cylinder (Figure 3.10 a)[12], which can be microns in length but only a few nanometers in diameter. Such a high aspect ratio structure is always the ultimate goal for AFM tips. SEM picture of AFM probe with CNT tip is shown in Figure 3.10 b[12]. The carbon nanotube is born to be a high aspect ratio tip that is capable of more accurate imaging of structures with steep sidewalls such as gratings. The small size in diameter promises significantly less tip-sample adhesion[13], which results in less potential sample damage during the imaging. Second, carbon nanotubes

are very stiff and has extremely large Young's modulus. In 1999, a 1.0-1.5nm diameter single-walled carbon nanotube has been studied and revealed a Young's modulus of 1.25TPa[14], which makes CNT the material stiffer than any other known materials. Impressive durability of CNT tips can be expected. Last but not least, CNT tip is able to buckle elastically under large loads. After suffering from heavy loads, the carbon nanotube can return to its original configuration as long as tip is away from the sample. Experiments demonstrated that CNT can even be bent close to 90℃ many times without noticeable damage[15] and thus is supposed to be a wonderful material for ultimate robust AFM tips.

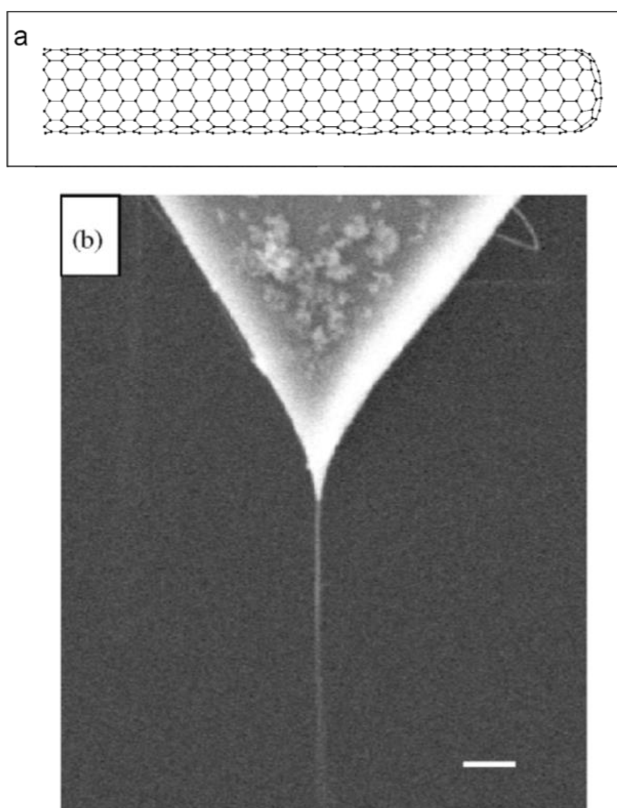

Figure 3.10 (a) The structure of a single-walled carbon nanotube. Each vertex corresponds to a sp^2-bonded carbon atom. (b) SEM image of an AFM probe with a CNT tip.[12]

The first carbon nanotube AFM tips were produced in 1996 by manually attaching multi-walled carbon nanotubes to normal pyramid-shape tips.[13] Unfortunately, tips with multi-walled carbon nanotubes generated in this way were unable to provide much improvements in resolution. Single-walled carbon nanotube tips are thus necessary. Later, metal-catalyzed chemical vapor deposition (CVD) took the place of attaching method to directly grow carbon nanotubes on normal tips.

Today, there are two general acceptable way of CVD to grow CNT on normal tips. The first is pore growth method. In previous studies, it was realized that CNT grew perpendicular to a porous surface containing embedded catalyst. Thus a flattened area is created first on the normal tip by high-load scanning on a hard surface (i.e. diamond). Then the tip is anodized in HF to create 100nm diameter pores in the flat surface. Next, iron was electrochemically deposited into the pores as catalyst particles. Tips prepared in this way were heated in low concentrations of ethylene at 800℃, which is known to favor the growth of thin nanotubes.[16] The process is also illustrated in Figure 3.11.

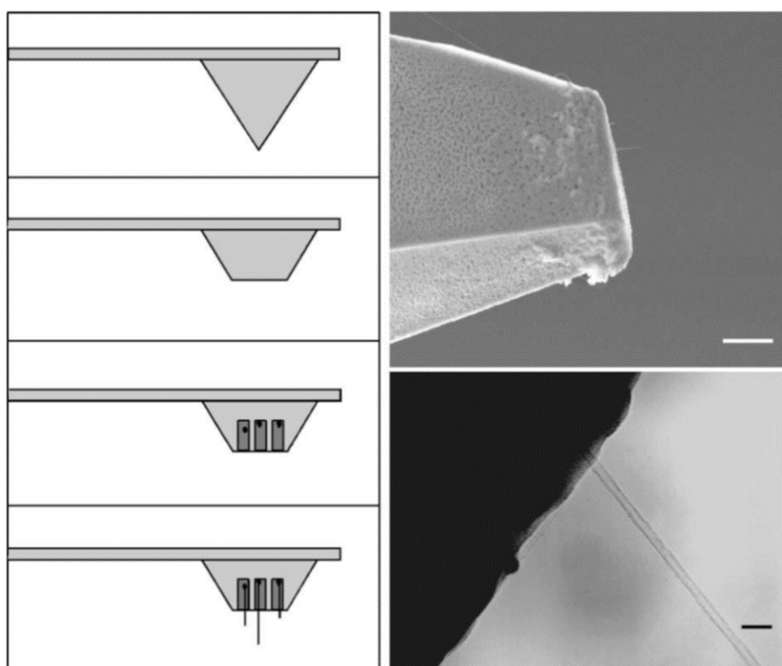

Figure 3.11 The pore-growth technique for CVD nanotube tip production: The panels on the left illustrate the steps involved in tip production: flattening, pore formation, catalyst deposition, and CVD nanotube growth. SEM (top right, 1mm scale bar) and TEM (bottom right, 20nm scale bar) of individual carbon nanotube tips produced by the pore growth method.[17]

The second is surface growth method. When a growing nanotube reaches an edge of the pyramid, it can either bend to align with the edge or protrude from the surface. The pathway followed by the nanotube is determined by a trade-off between the energy gain of the nanotube–surface interaction and energy cost to bend nanotubes. If the energy required to bend the tube and follow the edge is less than the attractive nanotube–surface energy, then the nanotube will follow the pyramid edge to the apex. As a result, nanotubes are steered towards the tip apex by the pyramid tip edges. At the apex, the nanotube must

protrude along the tip axis since the energetic cost of bending is too high.[12] A schematic of such method is shown in Figure 3.12.

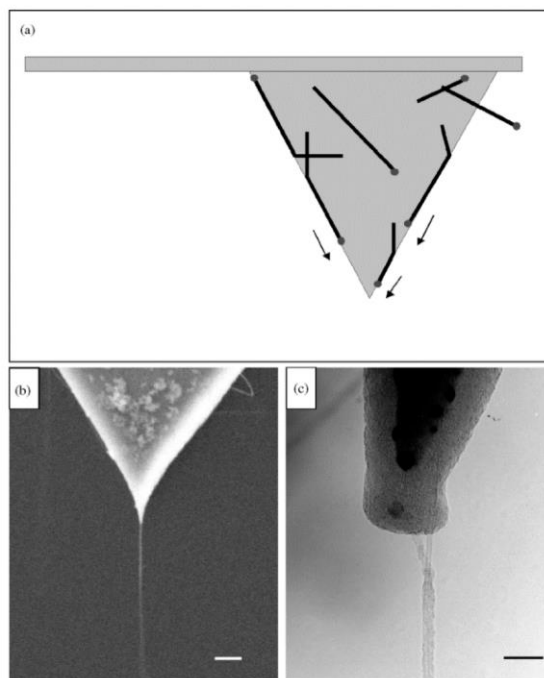

Figure 3.12 Surface growth method for CVD nanotube tip preparation: (a) Schematic illustration of surface growth process, where nanotubes grow on the pyramidal surface, guided along the edges towards the tip apex. (b) SEM and (c) TEM images of a single-walled nanotube surface growth tip consisting of two single-walled nanotubes.[18]

In conclusion, the carbon nanotube tips have showed great potentials and a promising future. Carbon nanotube is a desirable material that is able to solve the problem of both robust and sharpness simultaneously. But obstacles that prevent CNT tips to be broadly adopted are still remained to solve. The complexity of fabrication and high cost are probably two vital factors that needs much concern in the future.

3.6 Conclusion

AFM has been proven as a powerful tool to reveal the nanostructures and for many other applications. Nevertheless, all the current fabricating techniques have some restrictions that are not able

to get perfect AFM tips. Indirect method allows flexibility to choose the tip materials but lacks the sharpness of the tip. Direct method promises tip sharpness but lacks the tip versatility. And further sharpening is always necessary after both methods. On the other hand, investigations about carbon nanotube exhibited its great properties that are suitable for being the tip material. Even though obstacles exist in fabricating carbon nanotube tips, it is still worthy to looking for possible solutions to overcome them.

Chapter 4 Batch fabrication of Direct Positioning (DP) AFM tip

This chapter describes our way to fabricate the AFM probe with particular tip that is able to position upon the sample directly. Our process starts with regular pyramid-shape tip and its geometrical structure will be redefined in a simple and low-cost manner.

4.1 Shape of AFM tips

With more fabrication techniques available, AFM tips are no longer exclusively pyramid-shaped. A lot of tips with different shapes are commercially available nowadays for particular applications. For instance, because the normal tip with pyramidal shape has a large bottom, it can be hindered by the sidewall of a deep trench thus unable to reach the bottom if the width of the trench is very small. Therefore, some tips with special high aspect ratio shapes are fabricated for such specific application. It is well-known that AFM tips require extreme sharpness at most scenarios, but surprisingly, some tips with blunt shape are also highly demanded for hard contact between the sample and the tip. To be specific, nanoindentation exploits a large variety of tips with disparate shape to characterize the mechanical properties of thin films. In principle, if a very sharp tip indenter is used, the volume of material to be characterized can be extremely small, and therefore, rounded tips are always desired in nanoindentation.[1,2] Figure 4.1 shows SEM images of some AFM tips with different shapes.

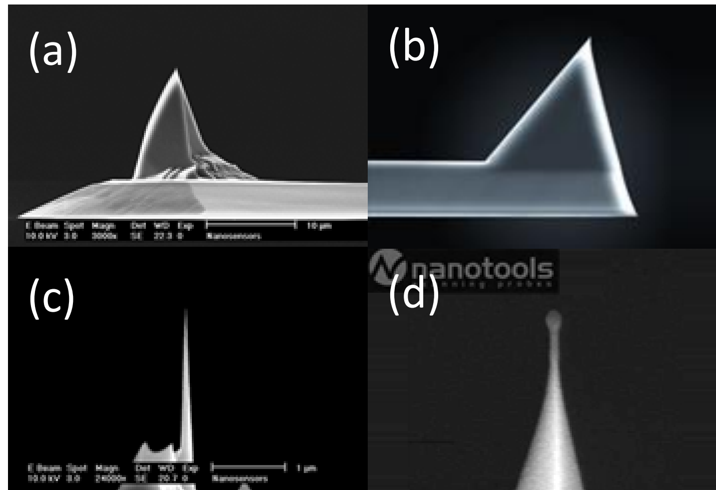

Figure 4.1 SEM images of tips with different shapes, (a) 4-side pyramidal tip (b) 3-side pyramidal tip (c) high aspect ratio tip (d) sphere-end tip. (SEM pictures courtesy to Nano Sensors, Nanotools, Nano World)[3]

In a word, the determination of the tip shape is purpose-directed and dependent on specific applications. In our particular case, the tip has a tetrahedral corner-like shape as shown in Figure 4.2. This specific shape is chosen so that the tip locates precisely at the very end of the cantilever. For a normal tip, it is impossible to know where exactly the tip is because the camera used in a AFM system only shows the backside of the AFM probe, which means that user must speculate an approximate range for the tip location. Figure 4.3 shows a picture of the tip captured by the built-in camera of an AFM system. The uncertainty of the tip location has raised up two major problems. First, the scanning field must be large to make sure that the area of interest is covered. Second, multiple attempts must be necessary before finally locates the area of interest. Such problems are especially worse when the area of interest is small, for instance, a few nanometers. Both problems will increase the risk of damaging the sample surface especially for soft samples. In order to get rid of these inconvenient problems, an AFM probe with the tip locating at the very end of the cantilever is desired. And our tip provides the feature of positioning upon the sample directly.

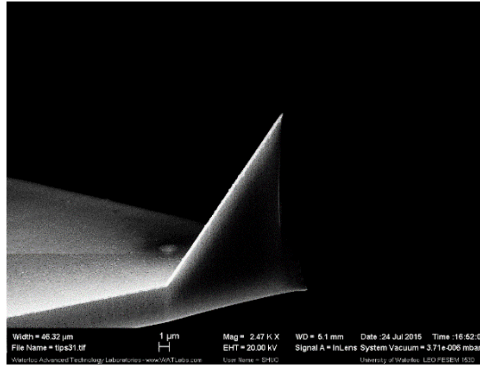

Figure 4.2 The SEM image of a corner-like DP tip made by our process.

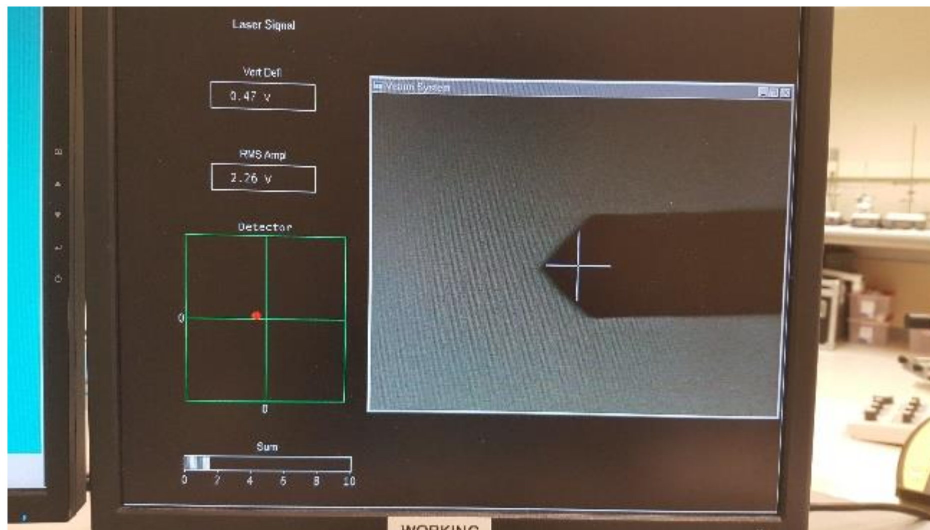

Figure 4.3 A picture of the probe captured by the built-in camera of Veeco AFM system. The cross mark refers only an approximate location of the tip.

4.2 Fabrication of DP AFM tip

Our process starts with a commercial AFM probe and modifies its shape to meet the requirement of an DP tip. The goal of the process is to make it simple, low-cost and applicable on multifold AFM probes. The basic logic behind our process is as follow: First protect the wanted region, and then modify the shape by removing the unwanted area and get rid of protective layer at last. Therefore, our process includes three general steps: Electron-beam evaporation, deep silicon RIE and wet etch. The details of these techniques have been introduced in Chapter 2.

4.2.1 Electron-beam evaporation of aluminum

To protect the desired region, it's natural to add a protective layer. This purpose is achieved by the evaporation of metals. As discussed in chapter 2.2, evaporation is a highly directional process. To avoid depositing on all surfaces of the tip, shadowing effect must be employed so that almost no deposition of protective layer occurs on the unwanted region. Thus we implement angled-evaporation method. In our case, the tip is required to be located at the end of the cantilever, which means the inner side of the tip is the desired region. Hence the angled deposition is carried out in the direction shown in Figure 4.4 (a). The sidewall of the tip blocks the incident evaporated metal atom to reach the other side of the tip and creates shadowing areas. Surprisingly, deposition in a "reverse" direction shown in Figure 4.4 (b) also works for our purpose. There will be a shadowing area on the cantilever and a hole can be formed after silicon RIE to show the exact tip location. Because the position of the source is set and impossible to change, we must provide an angle to the tips to achieve these angled depositions. In practice, the tips are always mounted onto a carrier wafer for batch fabrication so that it is much easier to handle. Therefore, we can attach the carrier wafer to a stub with certain angle as illustrated in Figure 4.5. Empirically, this angle is chosen to be 60° so that our deposition process works for most tips whose sidewalls have various steepness.

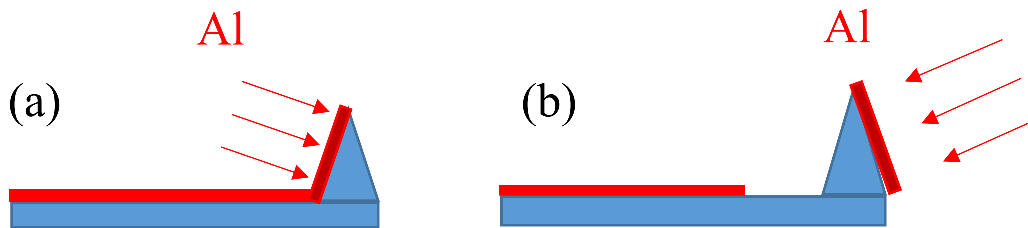

Figure 4.4 A schematic of angled deposition of aluminum. The blue areas represent the AFM tip and the red areas show the surface that will be covered by aluminum. (a) If aluminum is deposited in this direction ("front deposition"), little aluminum will be deposited on the outer side of the tip, (b) shadowing areas occur both on the cantilever and the inner sidewall of the tip once aluminum is deposited in this direction ("reverse deposition").

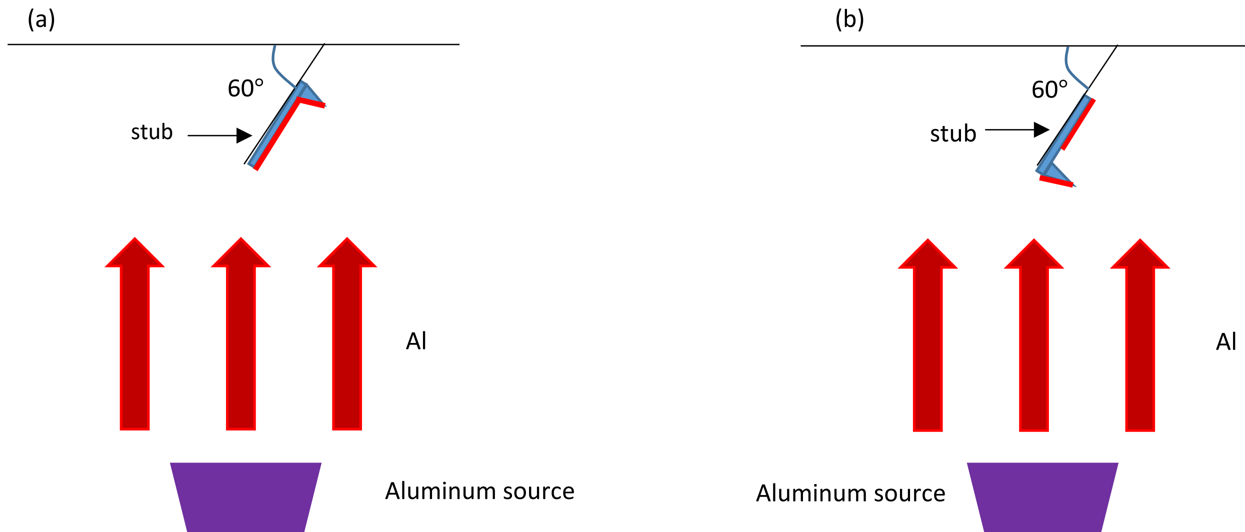

Figure 4.5 Actual setting in the deposition system. A stub of 60° is used to provide an angle so that the depositions described in Figure 4.4 (a) and (b) are carried out respectively.

There are several parameters we need to examine in this step. First is the metal that's used as the protective layer. Several requirements are necessary in determination of such metal. First, it should be low-cost and easy to get. Second, it must be simple to be removed by liquid chemicals. Last, it must have moderate or low stress so that the tip itself can be perfectly covered and protected. There are various metals that meet the first two requirements above but the last requirement plays a critical role in clinching the decision. The thin film deposited onto the tip creates two kinds of stresses. First is the extrinsic stress which is due to the sources external to the deposited film such as thermal induced stress during the evaporation.[4] Second is the intrinsic stress due to the properties of the film itself such as atom spacing, grain orientation and size, etc. The combination of these two kinds of stresses will finally determine the effect acting to the tip. At the beginning, we had two candidates: Aluminum (Al) and Chromium (Cr). They are both deposited onto the tip and results are examined. Figure 4.6 compares their results and effects acting to the tip can be explicitly observed. As a result, Cr tends to have large stresses so it curls up and leaves some regions of silicon unprotected. Meanwhile, Al is capable of depositing upon the tip without damaging it. Therefore, Al is finally chosen for our process.

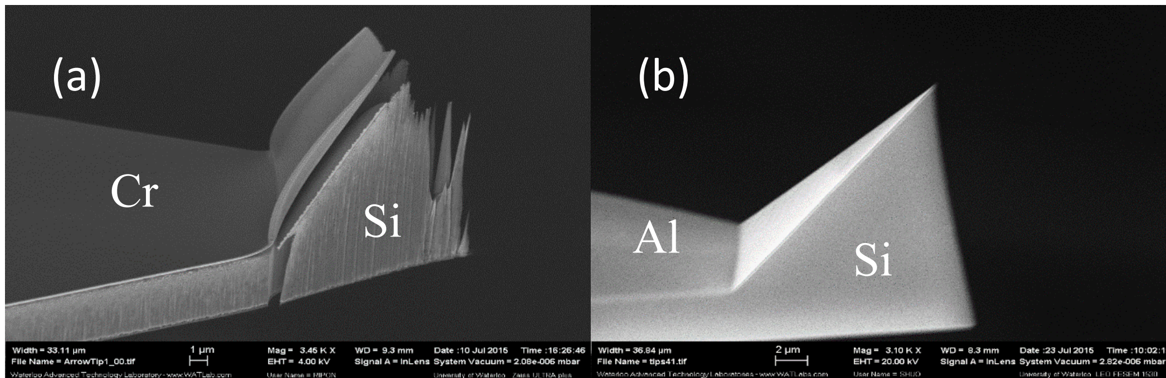

Figure 4.6 The SEM images compare the results of protective layer consisting of (a) Cr, (b) Al. It is clearly seen that large stresses distort the Cr layer and the unprotected regions of silicon are damaged during RIE in the next step. On opposite, Aluminum is competent to keep tip well-protected.

After determination of the material used for the protective layer, we have some other parameters in concern. First is the deposition rate. As discussed in Chapter 2, a high deposition rate is always preferable in theory. However, it is not always true in practice. In the case of Al, there might be air in the form of gas bubble trapped in the bulk Al source to make Al splash and it is then hard to get stable deposition. Therefore, we need to heat the Al slowly to the melting point, which amounts to low deposition rate at the same time. Tradeoff is hence made and finally we choose 2Å/s to be the standard deposition rate for our process. Second is the thickness of the deposited film. As mentioned above, we always mount tips onto a carrier wafer so that it is easier to handle. Thus there will be some small pieces of silicon, which are partially covered by photoresist, placed next to the tips on the carrier wafer. Then deposition will occur simultaneously on these silicon monitors and the tips. After deposition, photoresists on the monitor will be removed and a step can be revealed between the region once covered with the photoresist and those regions without the photoresist. One can measure the height of such step by surface profiler to get the real thickness of the deposition. Because Al we need is working as a sacrificing layer, the thickness can vary in a small range instead of an exact value as long as it is thick enough to protect the underlying tip. In practice, our target thickness of Al layer is 200∼240nm. The uniformity is another parameter we care. If the carrier wafer is a 4-inch silicon wafer, monitors are placed at different positions and thickness measured are proven to be residing in the range shown above. Therefore, the uniformity is verified as well. Figure 4.7 shows the successful results after this step.

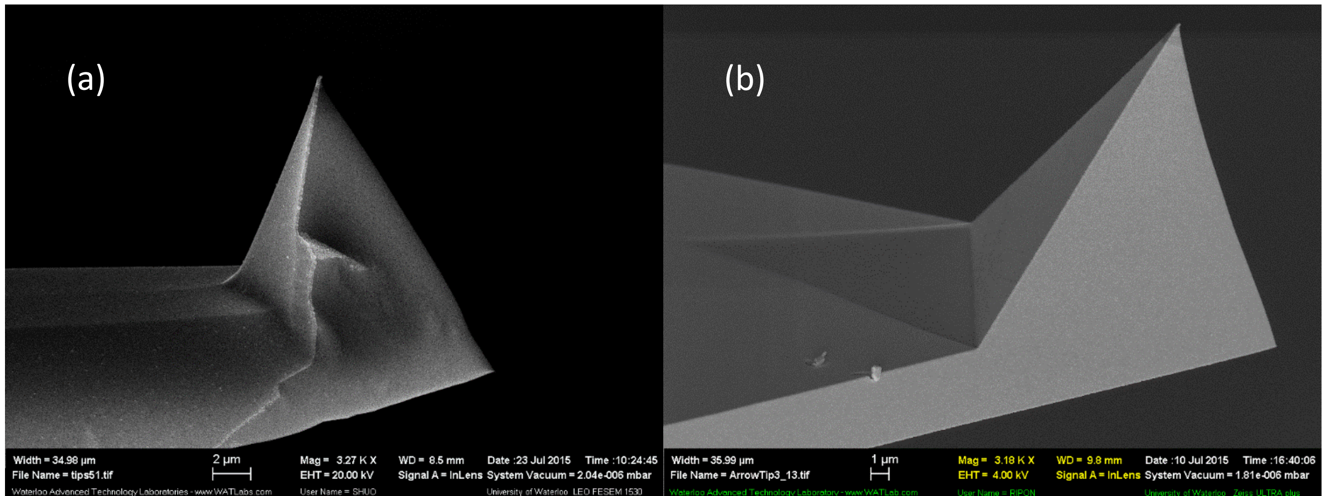

Figure 4.7 SEM images of (a) “front deposition” achieved on an ACT tip, clear edge of Al is observed and (b) “reverse deposition” on a 3-sided pyramid tip, clear shadowing area is shown.

4.2.2 Deep Si RIE (DRIE)

We want the tip locating exactly at the end of the cantilever, which means that the outer sidewall of the tip needs to be strictly vertical. Such vertical sidewall is highly directional, which needs anisotropic etching. This is the reason why this step is carried out by Si RIE. As explained in Chapter 2, etching profile is highly dependent on the gas contents in the plasma. Hence the first task is to ensure the “recipe” that is able to acquire this vertical sidewall. The most famous recipe for DRIE is probably the Bosch Process.[5-7] However, Bosch Process is working in a mechanism alternating polymerization and etching all the time, so the sidewall always has wave-like profile. To obtain smooth sidewall, a pseudo-Bosch process is often implemented in practice. In our case, the recipe name for such pseudo-Bosch process is “Temp-Reza-2” developed by Dr. Reza. This recipe employs a gas combination of C_4F_8 and SF_6 just like Bosch process does. However, without switching the gas, they are constantly supplied with a desired ratio. This ratio turns out to be the most important parameter to control the etching profile. The relation between the gas combination ratio and the etching profile has been investigated by some groups already.[8] In order to get a vertical profile, the ratio is set to be C_4F_8/SF_6 = 38/22.[8] Once we determine the etch recipe, it also means that the etch rate is determined as well. For this particular recipe, the etch rate is 400$\pm$10 nm/min for Si. Fortunately, the etch rate for Al by using this recipe is more than 100 times slower, which amounts to a wonderful selectivity between Si and Al. Because the thickness of our protective layer (Al layer) is around

200nm, the maximum etch duration is then around 50 minutes so that the protective layer can still be functional. Next parameter in concern is the depth we need to etch in total. In most scenarios, AFM tips often have a height smaller than $8\mu m$ and cantilever thinner than $4\ \mu m$. Therefore, we set the etch duration to be 20 minutes, which is not only enough for our process but also smaller than the maximum etch duration shown above. Our target in this step is to etch the tip all the way down to the bottom if Al protective layer is front-deposited, or etch through the cantilever and create a whole if Al protective layer is reversely deposited. Figure 4.8 shows the results we obtained for both cases.

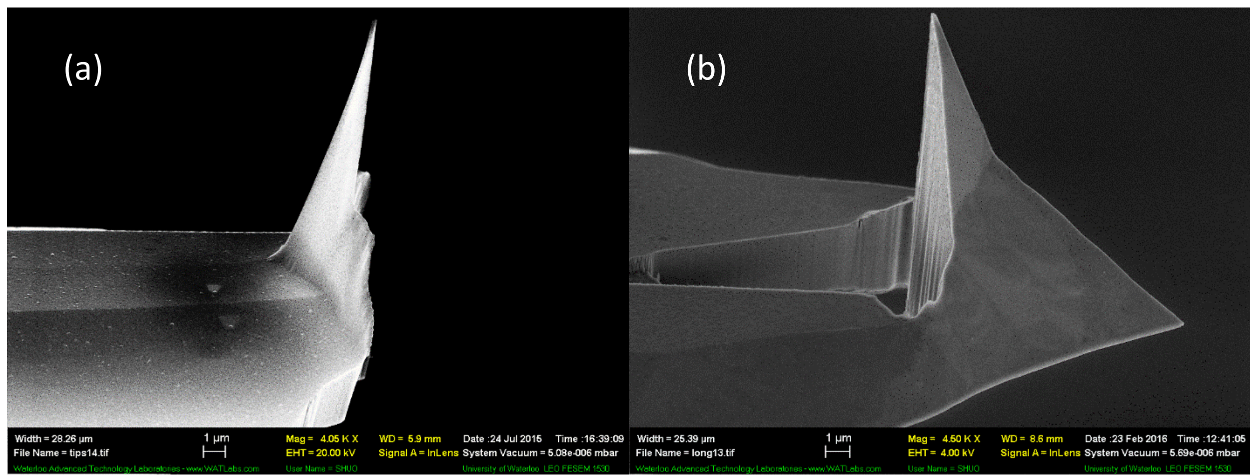

Figure 4.8 SEM images for the etch results of (a) ACT tip that has undergone “front deposition” and (b) 4-sided pyramid tip that has undergone “reverse deposition”.

In theory, we don’t need to do anything special after DRIE. Nevertheless, we need to apply an extra Oxygen Plasma etching to the tips in reality. The polymerization acquired in DRIE (discussed in Chapter 2) might have some residue lying on top of the Al layer, affecting the wet etch in next step. Oxygen Plasma works in such a manner that it burns out the polymer layer, and hence helps to remove these residues.

4.2.3 Al wet etch

As discussed in the previous chapter, wet etch is the oldest etch technique which is cheap and easy to implement but comparatively hard to control the results. Nevertheless, Al is only working as a protective layer in our process, which means no pattern transfers onto it occur. We only need to make sure that Al is

completely removed and no negative effect acting to the Si underneath. Therefore, the advantages of wet etch are maximized while the drawback is almost neglectable.

The very extensively used Al etchant is PAN. At the beginning, it was our option to etch the Al as well. However, we find out that hydrofluoric acid (HF) can be a good replacement for our process. There are two issues for PAN. First, PAN is not working well at room temperature while HF is working in comparatively low temperature. PAN has to be heated up to around 40~50℃ to start etching. Second, the etch rate for PAN is slower compared to that of HF. Although HF attacks oxidized silicon, it has no effect on silicon itself or any other materials used in our process. Therefore, we finally decided to use HF instead of PAN. The first parameter we care is the etch rate of HF. Obviously, the etch rate of HF is related to its concentration. In practice, we tried 1:20 diluted HF. There are two ways to measure the approximate etch rate. First, deposit a thin layer of Al onto a transparent glass and dip it in HF. A visual test can then be finished to measure an approximate etch rate. Second, coat photoresist partially onto an Al surface and immerse it in HF for a short duration such as 5s or 10s. Then photoresist will be removed and a step structure will be revealed. Then we can get the etch rate by dividing the depth measured by the duration. Both methods can only get an approximate etch rate which seems problematic in theory. Empirically, however, we always double the etch duration to achieve an over-etch to ensure the wet etch is complete. So in fact, the etch rate we get in either way is feasible. In our experiment, 1:20 diluted HF is able to thoroughly remove 200 nm Al in 1 minute, namely an etch rate around 200nm/min. Thus finally, we set the standard etch duration to be 2 minutes. HF with higher concentrations are also applicable and the etch duration needed is supposed to be shorter. Figure 4.9 compares successful and failed results after removing Al protective layer on tips.

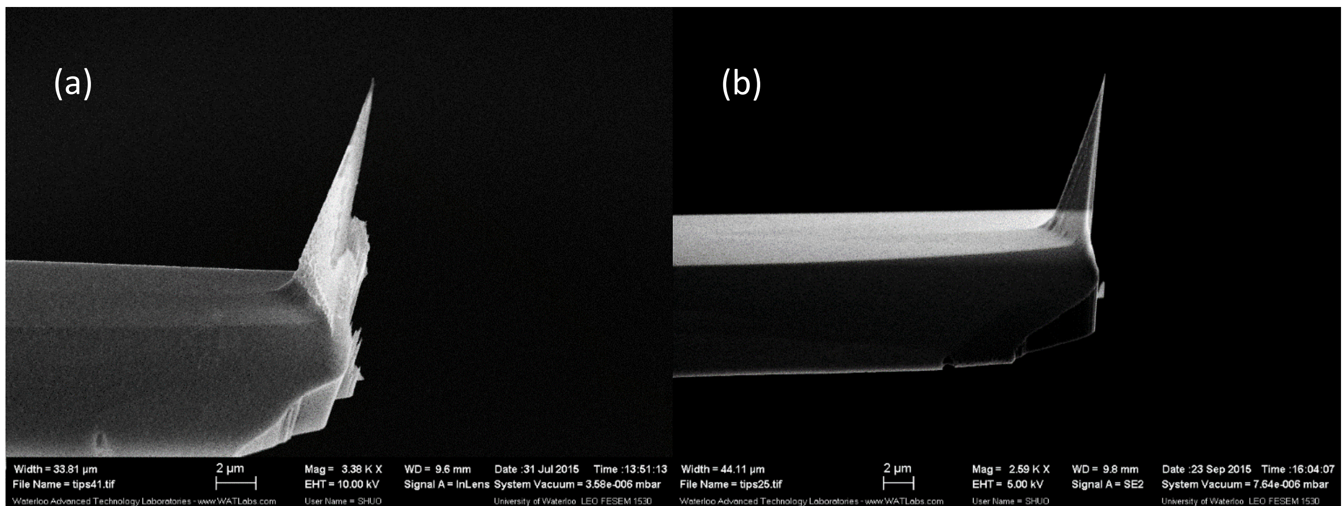

Figure 4.9 SEM images of (a) AFM tips with incomplete HF wet etch, clear Al residue can be observed, (b) tips with clean and sufficient HF wet etch.

4.3 Results, discussion and concluding remarks

Our process provides a simple and cheap way to fabricate tips with the ability of direct positioning. The tip can be located either at the very end of the cantilever or besides the hole as shown in Figure 4.10. Other than the simplicity and the low cost, it also offers the feasibility to tips with disparate shapes, as exhibited in Figure 4.11. Moreover, since the dimension of the tip is significantly decreased in one direction, it has potential to be used as high-aspect-ratio (HAR) tip in some certain situations.

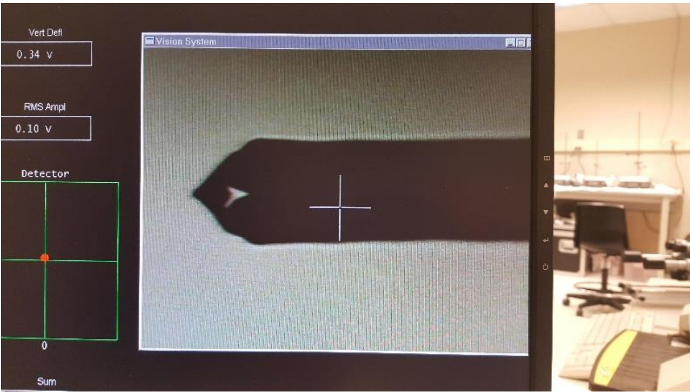

Figure 4.10 An image of the backside of a tip made by our process captured by the built-in camera. There is a clear hole on the cantilever near which the tip locates.

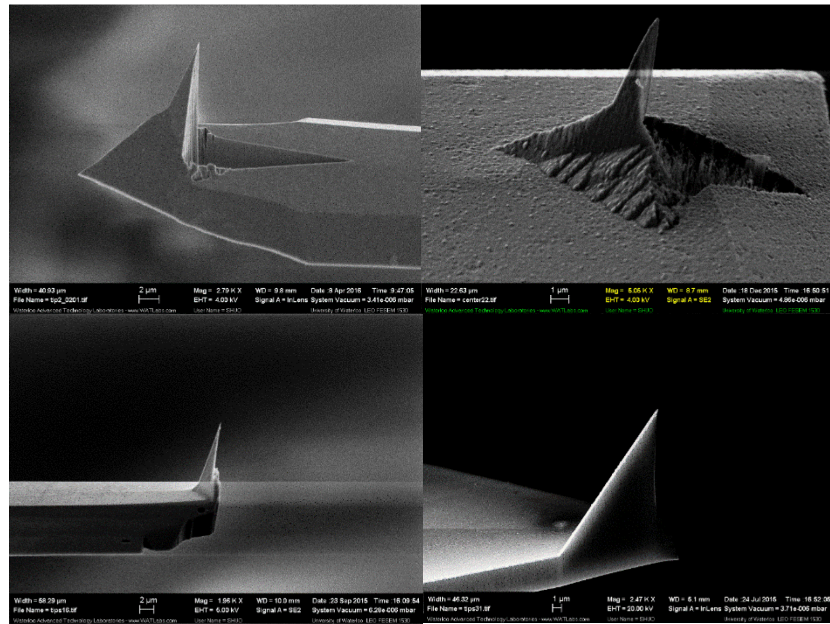

Figure 4.11 An exhibition of tips with various shapes made by our process. The feasibility of our process to different tip surfaces is confirmed.

On the other hand, our process does have some disadvantages. First, the original AFM probes that are used need to have a high quality. The shape of our product is highly dependent on the original shape of the tip. Original tips with bad profile might lead to weird products as depicted in Figure 4.12. Even with potential of being HAR tip, the major feature of the tip we fabricated is still the ability of direct positioning. The reason is that our tip reaches a high aspect ratio only in one dimension. Figure 4.13 shows the SEM images of the same tip viewed from lateral and back side. Obviously, the dimension in the cross-sectional direction is still very large. Test results (shown in Figure 4.14) acquired by our fabricated tip scanning the high density pillars prove that our tip can only reach the bottom in some certain direction. However, for some strongly regulated structures like gratings, our fabricated tip might be able to meet the demand.

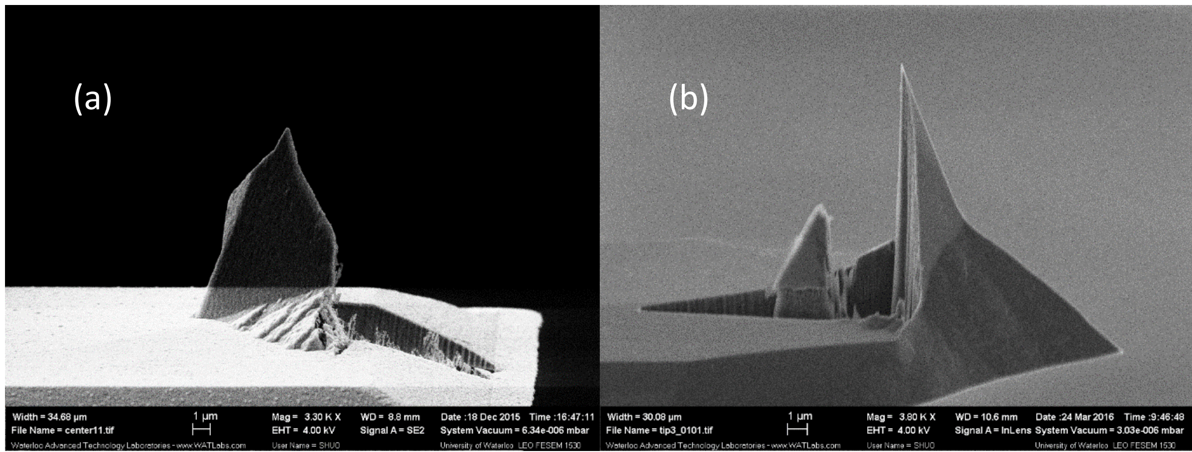

Figure 4.12 SEM images of random shape obtained due to the bad quality of the original tip.

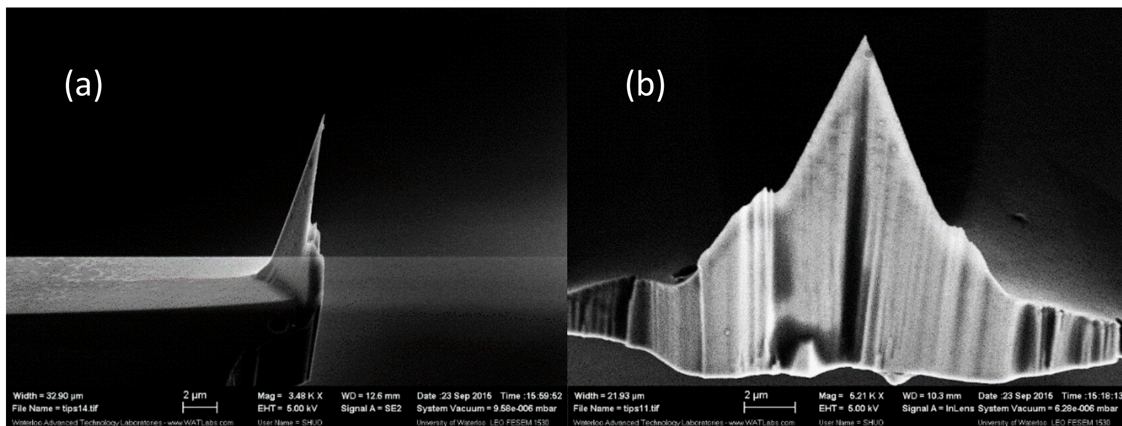

Figure 4.13 The SEM images of the same tip captured in (a) lateral side and (b) backside. It is clearly seen that the dimension decreases significantly in one direction but remains the same in the other direction.

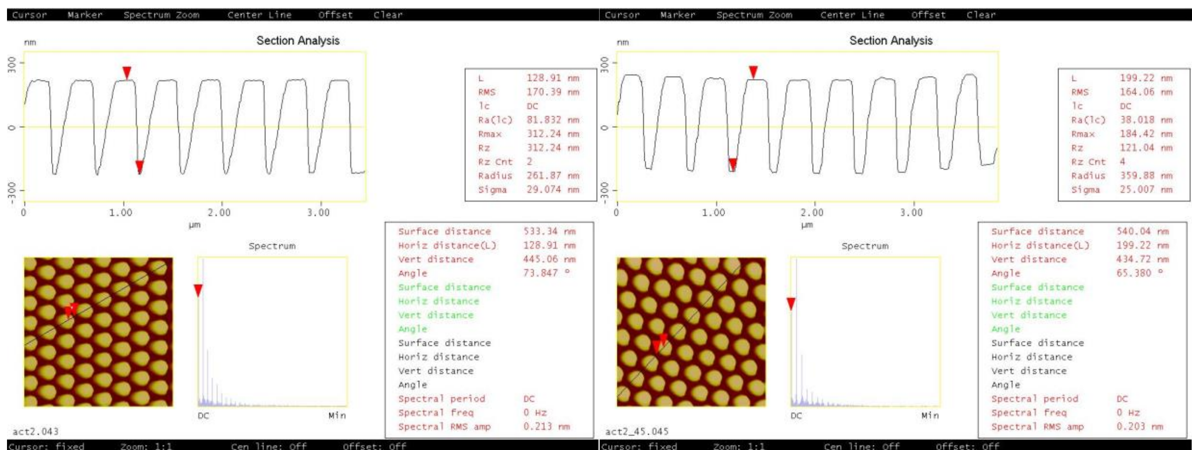

(a) (b)

Figure 4.14 Screenshots of a fabricated tip scanning high-density pillar arrays. (a) The tip scans in a random direction but hard to reach the bottom at most regions, (b) the tip scans in a direction perpendicular to the previous one and reaches the bottom in all regions.

Chapter 5 Mixture of ZEP and PMMA with varying ratios for tunable sensitivity as a lift-off resist with controllable undercut

This chapter is not related to the previous chapters and starts a new topic about a novel way to construct a bilayer system for lift-off process. Our method exploits the close connection between the mixture ratio in a ZEP/PMMA composite and its sensitivity to offer the ability of controlling the size of the undercut. This work is published in Journal of Vacuum Science & Technology B.[1]

5.1 Introduction

A lift-off process is a popular method to pattern metals, especially for the noble metals that are hard to dry-etch. In a lift-off process, a pattern is first defined in the resist using lithography. Then a film of desired metal is blanket-deposited all over the substrate. Finally, the resist is dissolved and the metal on top of it is thus lifted off, leaving behind metal structure that is originally in contact with the substrate. Yet when the material to lift-off is sensitive to solvent or liquid (*e.g.,* organic conducting material), it is also possible to carry out a "dry lift-off" process without using any liquid.[2] An undercut profile (*i.e.,* opening is widest near the bottom) is always desirable in order to obtain a clean lift-off[3-6] because the undercut assures that the metal on top of the resist is disconnected to that in contact with the substrate. If the undercut is large enough, a less directional deposition method such as sputtering can also be used for lift-off process, and the metal to lift-off can be very thick.

Various techniques have already been developed to attain an undercut profile. Slight undercut can be obtained using a single layer resist exposed by a low energy electron beam. For positive tone resist, single layer poly (methyl methacrylate) (PMMA) was reported to successfully create an undercut profile when exposed at a low energy of 3 keV that leads to more electron forward scattering than high energy exposure.[7] For negative resists, lift-off is rarely used for pattern transfer because a slightly positively tapered profile, instead of an undercut profile, would usually result because of electron forward scattering.

Nevertheless, lift-off using the negative resist such as polystyrene[8] or water soluble poly (sodium 4 styrenesulfonate)[9] can be realized when using very low energy exposure such that the resist bottom is inadequately exposed and thus dissolves fast in the developer. It is important to point out that, for lifting off some structures such as nanoscale trenches or holes, a negative resist is preferred as it offers far less exposure time than positive resists (yet a complicated double lift-off process using a positive resist can be employed to obtain such structures[10]).

A robust large undercut profile can be more readily achieved by using bi-layer or tri-layer (resist/hard mask/polymer) film stacks. For the case of bi-layer, the bottom polymer could be either a resist having a different sensitivity than the top resist layer when developed using the same developer as the top layer or a different developer, or a non-resist that can be wet-etched using an etchant that will not attack the top resist layer. When both layers are positive e-beam resists, during exposure the proximate areas (that are not directly exposed) are exposed by the backscattered electrons, and such a proximity effect leads to a lateral extension of the structure. The extension is largely dependent on the exposure dose and sensitivity of the resist. When the exposure dose is fixed, the sensitivity difference between the two resists determines the amplitude of the lateral extension/undercut.

One of the most widely employed bi-layer systems is a positive resist over a so-called liftoff resist polydimethylglutarimide (PMGI) or LOR (consists of mainly PMGI).[11] PMGI is soluble in base solutions such as common developer for photolithography with greatly increased solubility upon electron beam exposure,[6, 12] but after being well baked it becomes insoluble to most acids and organic solvents including common solvent developers for positive e-beam resists. The amplitude of undercut can be controlled by adjusting the soaking time in the base solution that dissolves PMGI without attacking the top organic resist layer. However, wet chemical etching is generally not well reproducible and the amount of resulted undercut depends greatly on the opening in the top resist layer, with larger undercut for wider opening. Interestingly, it is found that solvent, particularly those used for developing PMMA including diluted methyl isobutyl ketone (MIBK), diluted methyl ethyl ketone (MEK) and 2-ethoxyethanol (cellosolve), can also be used to develop PMGI with the sensitivity a few times lower than that of PMMA.[13] As such, a double layer consisting of a PMGI top layer and a PMMA bottom layer can be used to attain a large undercut profile using the common developer for both resists.

In addition, a film stack of high molecular weight (Mw) PMMA/low Mw PMMA can provide a certain degree of undercut profile since the low Mw PMMA has higher sensitivity than the high Mw one. Yet for the chain scission resist, the dependence of sensitivity on Mw is very weak, because for longer

chains, though more chain scission is needed to render it soluble in the developer, it also receives proportionally higher exposure dose. For instance, when Mw is decreased from 2200 to 50 kg/mol, PMMA's sensitivity increases by only 26%.[14] This weak dependence limits the achievable undercut. Alternatively, a copolymer of PMMA-co-PMAA (poly (methacrylic acid)) can be used as the under-layer as it is more sensitive than the top layer PMMA. ZEP can also be used as the bottom layer under PMMA as it is more sensitive than PMMA,[15] but the undercut would be often too large since ZEP is about 3 times more sensitive than PMMA. Alternatively, fullerene can be added into ZEP resist to make it less sensitive, and thus a bi-layer resist stack consisting of a fullerene-incorporated ZEP top layer and pure ZEP bottom layer can offer a large undercut profile.[16] For the ZEP resist (as the top layer), besides LOR, PMMA has also been employed as a bottom layer that is more sensitive than ZEP when using undiluted MIBK as developer.[5] Lastly, hydrogen silsesquioxane (HSQ) over PMMA has been employed successfully for lift-off, with the undercut profile created by excessive lateral etching of PMMA by oxygen plasma with the exposed HSQ (becomes effectively SiOx) as hard mask.[17]

For the bottom layer, a resist with tunable sensitivity is apparently the most desirable, as it can offer a controlled amount of undercut. Ideally, a large undercut profile is preferred to enable the lift-off of very thick metals. But too large undercut may lead to the collapse of the top resist layer onto the substrate, and the situation gets worse for dense structures. With tunable sensitivity, the amount of undercut can be adjusted according to different applications in order to achieve an optimal lift-off process.

In principle, since the sensitivity (μC/cm2) for negative resists like polystyrene is inversely proportional to its number averaged molecular weight (Mn),[18,19,20] one can achieve an undercut profile using a bi-layer with the bottom layer having a lower molecular weight than the top one, and the relative sensitivity thus the amount of undercut can be tuned readily by choosing the appropriate Mn of the two layers. Though the exposed polystyrene becomes insoluble in common solvent because of the chain cross-linking, a hot mixture of NH4OH, H2O2 and H2O (RCA-1) can be used to dissolve it for lift-off. Unfortunately, despite our great effort, we were not able to find a solvent that can dissolve polystyrene for spin-coating without dissolving significantly the bottom polystyrene layer during spin-coating of the top layer. This is contrary to positive resists like PMMA and ZEP, which doesn't dissolve significantly (less than ~30 nm if the bottom resist layer is well baked, and the dispersion and spin-coating of the top resist is carried out quickly within 1 min).

In this study, we will show that a simple mixture of PMMA and ZEP can offer tunable sensitivity by adjusting the volume ratio of the two resists both dissolved in anisole. The mixture can be used as the

bottom layer under PMMA, in order to obtain a controlled undercut profile for easy lift-off. Besides lift-off that is the subject of the present study, such a resist mixture having adjustable sensitivity can also be utilized to fabricate complicated quasi-3D structures mimicking Morpho butterfly scales using many layer resist film stacks,[13,21] or an imprint mold for a dual damascene process to fabricate Cu interconnect for integrated circuit.[22]

5.2 Experimental

PMMA (996 kg/mol) and CSAR-62 (a low-cost replacement of ZEP resist from AllResist Inc., and hereafter we still refer it as ZEP resist) were mixed together. As we do not have dry ZEP resist (as-purchased resist is already dissolved in anisole), we cannot mix dry ZEP with PMMA powder at a given weight ratio. Instead, we prepared PMMA solution in the anisole at a certain concentration such that it gave the same thickness as ZEP under the same spin-coating condition, and we assume this PMMA solution has the same weight concentration as the as-purchased ZEP. Then we mixed this PMMA and ZEP solution at various volume ratios (PMMA: ZEP = 0:1, 1:2, 1:1, 2:1, 1:0). For spin-coating the bi-layer film, we first coated the mixture resist, followed by baking at 120℃ for 10 min to drive off the solvent. Baking at a higher temperature and/or for a longer time might lead to undesirable phase-separation of PMMA and ZEP. Then we quickly coated the PMMA on top of the mixture film and baked it at 120℃ for very short time to minimize inter-mixing between the two layers. During spin-coating the top layer, the bottom layer was dissolved by ~30 nm that is acceptable since each layer was close to 250 nm thick.

Next, the bi-layer resist was exposed using LEO 1530 SEM equipped with NPGS pattern generation system at 20 keV and 0.8 to 5 nC/cm line dose. After the exposure, the resists were developed in amyl acetate, a common e-beam developer for ZEP yet also a good developer for PMMA, for 1 min. Finally, 100 nm Cr was evaporated and then lifted off by dipping the samples into the anisole for about 10 min, followed by ultrasonic agitation for 15 seconds in the same anisole solution.

5.3 Results and discussions

5.3.1 Contrast Curves

In order to confirm our assumption that the mixture resist's sensitivity can be tuned by adjusting the ratio of the two resist components, we first measured the mixture resist's contrast curves using AFM, which is plotted in Figure 5.1, together with the contrast curves for the pure ZEP and pure PMMA resist under the same development condition. For the contrast curves measurement, a single layer of pure or mixture resist was spin-coated with thicknesses of approximately 250 nm. As expected, higher PMMA/ZEP ratio leads to lower sensitivity (higher clearance dose). The clearance dose for pure ZEP resist exposed at 20 keV is 42 μC/cm2 with a contrast of ~7. The sensitivity is close to typical values reported in the literature. But for pure PMMA, it is considerably more sensitive with a clearance dose of only 61 μC/cm2 than typical values (~200 μC/cm2) obtained using the common MIBK:IPA (isopropyl alcohol) = 1:3 developer, suggesting that amyl acetate is a stronger solvent developer than diluted MIBK.

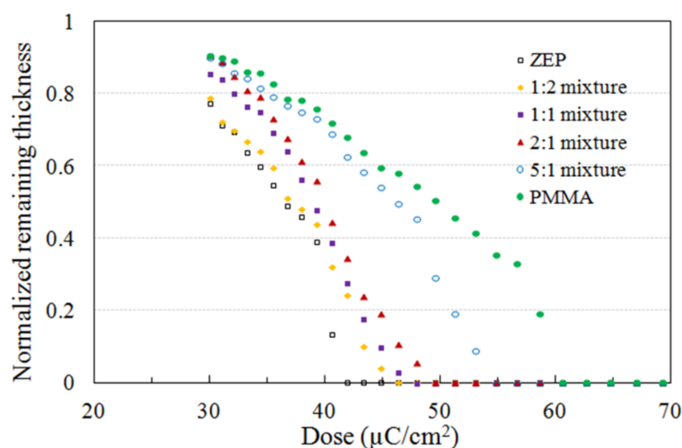

Figure 5.1 Contrast curves for the PMMA-ZEP mixture resist, as well as for pure PMMA and ZEP resist. The resists were exposed at 20 keV and developed in amyl acetate for 1 min. The ratios in the graph were volume ratios of PMMA: ZEP.

However, the resist's property is apparently dominated by the more sensitive resist (here ZEP) in the mixture. For instance, the mixture of PMMA: ZEP=2:1 has a contrast curve closer to that of pure ZEP resist than to pure PMMA even though it contains more PMMA. This property can be explained by the fact that PMMA molecular chains are not entangled with other PMMA chains and attached to a solid substrate; instead, it is embedded in the ZEP matrix. Thus once ZEP becomes soluble in the developer, the PMMA (though still with long chain) will be lifted off and effectively dissolved in the developer. This

result implies that one has to use a mixture with a very high PMMA/ZEP ratio in order to achieve a contrast curve lying near the middle of the two contrast curves for the two pure resists. For instance, the contrast curve for the 5:1 ratio lies near the middle of the two contrast curves for the two pure resists, though at lower doses it is closer to the contrast curve of pure PMMA because, at such low doses, the ZEP is not very soluble and the PMMA dominates the development process due to its much higher concentration in the mixture. Nevertheless, for our purpose, the lateral undercut is determined by the portion of the contrast curves with low exposure dose by backscattered electrons (*e.g.,* a dose of ~35μC/cm2 in the contrast curves), rather than the dose at clearance. As seen, at such low exposure doses, the amount of resist developed depends significantly on the ratio of the two resists in the mixture; thus the amplitude of undercut in the bi-layer resist system can be adjusted effectively by using different ratios without the need for very high PMMA/ZEP ratio.

5.3.2 Resist profile and lift-off of thick Cr

Undercut profile is greatly desired for a clean lift-off process. In order to verify the correlation between the resist sensitivity for the bottom layer and the amplitude of undercut, we exposed the bi-layer resist with periodic line-array structures. The top layer was pure PMMA and the bottom layer was the mixture of PMMA and ZEP or pure ZEP resist. The lines were exposed with single pass line pattern with varying line doses (unit nC/cm). Because of electron forward scattering and backscattering, the line-width increases with line dose and can go far beyond the electron beam spot size. Figure 5.2 shows the resist profile after development in amyl acetate. Figure 5.2 a-b are structures with a line array periodicity of only 200 nm exposed at a line dose of 1.32 nC/cm at 20 keV, with the bottom layer respectively of PMMA: ZEP = 2:1 and pure ZEP. This dose is determined as the optimal dose as it is high enough to expose the top (less sensitive) PMMA layer, and at the same time gives a reasonably large undercut without resist structure detachment when using PMMA: ZEP = 2:1 as the bottom layer. The undercut profile is evident for the mixture resist bottom layer, with some lines collapsed because of capillary force that becomes significant when the resist structure height is larger than its width. However, when the bottom layer is pure ZEP that has higher sensitivity than the mixture resist, the lines were all detached because the undercut was so large that they nearly merged together.

Figure 5.2 c-f are line arrays with a larger array periodicity of 500 nm, all exposed with an optimal line dose of 1.77 nC/cm at 20 keV. The dose is higher than the optimal dose for 200 nm array periodicity (1.32 nC/cm) because of lower pattern density and thus less contribution from proximity exposure. Again, the top layer is PMMA and the bottom layer is respectively a PMMA: ZEP ratio of 2:1, 1:1, 1:2 and 0:1 (pure ZEP). Clearly, the amplitude of the undercut increased with the amount of ZEP in the mixture. For a PMMA: ZEP ratio of 2:1 and 1:1, the amount of undercut was very close (70 nm and 75 nm, respectively), since their contrast curves nearly overlapped at low dose region of <40 μC/cm2 as shown in Figure 5.1. The undercut increased quickly to 104 nm for the 1:2 ratio mixture. When pure ZEP was used as the bottom layer, most resist lines were detached because of too high or even merged undercut.

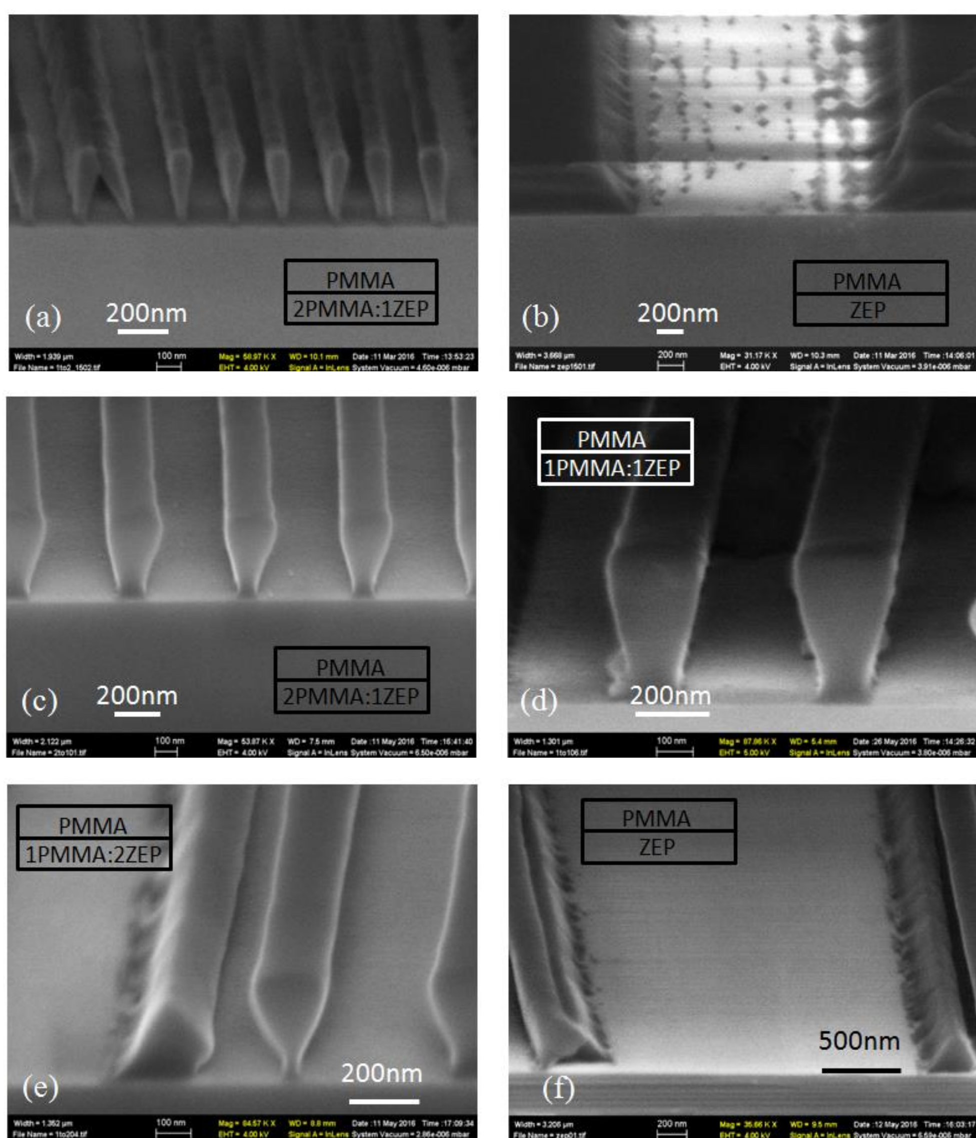

Figure 5.2 Line array resist structures after electron-beam exposure and development using amyl acetate for 1 min. (a-b) 200 nm array periodicity. (c-f) 500 nm array periodicity. The top layer is PMMA, and the bottom layer has a PMMA: ZEP volume ratio of 2:1, 1:1, 1:2 and 0:1 (pure ZEP). The lines collapsed or detached for (e-f) because of capillary force when the undercut was too large or even merged together.

For lift-off study, 100 nm Cr, which is pretty thick for lift-off, was deposited by electron-beam evaporation on the resist structure with 500 nm array periodicity, and then lifted off in anisole. Figure 5.3 shows the resulted Cr line array structures. As expected, best lift-off result was obtained for the PMMA: ZEP = 2:1 ratio (Figure 5.3 a). For the resist mixture with higher ZEP content (Figure 5.3 b-d) and thus higher sensitivity and larger undercut, either very wide Cr lines because of merged adjacent lines caused by too large undercut, distorted Cr lines, and/or unsuccessful lift-off (Cr on top of PMMA is not lifted off because of the resist structure falling down when the undercut is too large), are evident.

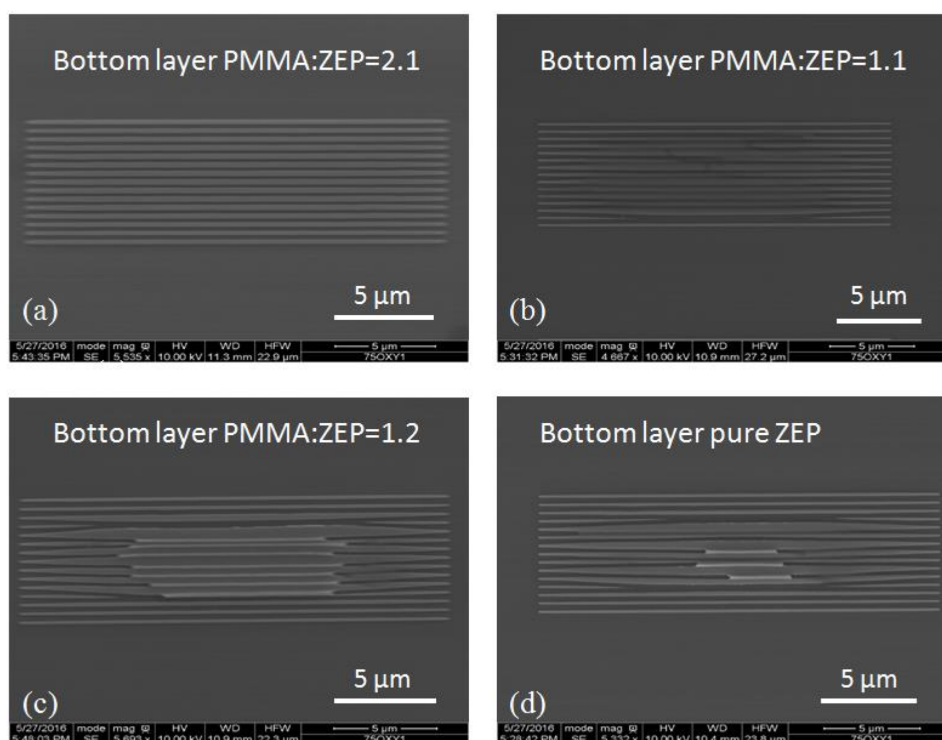

Figure 5.3 Cr line arrays with 100 nm thickness and 500-nm-array periodicity fabricated by lift-off using the bi-layer resist, consisting of top PMMA layer and bottom PMMA: ZEP mixture with the volume ratio of 2:1 (a), 1:1 (b), 1:2 (c), and 0:1 (pure ZEP) (d).

5.4 Conclusions

We studied the exposure property of the PMMA: ZEP mixture resist. The mixture behaved like the typical positive resist without noticeable micro-phase separation. The resist sensitivity increases with the content of ZEP in the mixture since ZEP is much more sensitive than PMMA; and the contrast curve of the mixture resist is closer to that of ZEP than to PMMA even with a PMMA: ZEP ratio of 2:1. With tunable sensitivity, the mixture resist is ideal for lift-off when used as the bottom layer, with the top layer being PMMA. The amplitude of undercut for such a bi-layer resist was adjusted readily by choosing different PMMA: ZEP ratios. However, though large undercut is desired for lift-off, too large undercut made the resist lines susceptible to collapse because of capillary force. With even larger undercut (by using pure ZEP as the bottom layer), the undercut of adjacent line structures merged together for 200-500 nm period line arrays, and the resist lines were thus completely detached after development. A moderate undercut obtained using PMMA: ZEP=2:1 as the bottom layer gave a well-defined resist line structure with array periodicity of 200 nm or 500 nm. This moderate undercut also resulted in the best result for the lift-off of 100 nm Cr. Larger undercut would be more suitable for larger (well beyond 500 nm) array periodicity.

Our technique has two main advantages. First, PMMA and ZEP are kinds of the two must have resists in most labs particularly with the recent introduction of low-cost ZEP replacement from various suppliers. Second, our technique is more reliable than using PMGI or LOR as the bottom layer, as the latter requires precise control of the wet etching time for dissolving the bottom layer.

References

Chapter 1

[1] http://www.nano.gov/nanotech-101/what/definition

[2] Saini, R; Saini, S; Sharma, S, "Nanotechnology: The Future Medicine". Journal of Cutaneous and Aesthetic Surgery. 3 (1): 32–33, (2010).

[3] "The size of things"- exposed by National Cancer Institute, http://nano.cancer.gov/learn/understanding/

[4] Gates BD; Qiaobing Xu; Stewart M; Ryan D; Willson CG; Whitesides GM, "New approaches to nanofabrication: molding, printing, and other techniques". Chemical Reviews. 105(4):1171-1196, (2005).

[5] Linjie Li; Rafael RG; Gershgoren E; Hwang H; Fourkas JT, "Achieving λ/20 Resolution by One-Color Initiation and Deactivation of Polymerization". Science. 324:910 (2009).

[6] Schmid GM, et al. "Step and flash imprint lithography for manufacturing patterned media". Journal of Vacuum Science and Technology B. 27:573 (2009).

[7] Lee KB; Lim JH; Mirkin CA. "Protein Nanostructures Formed via Direct-Write Dip-Pen Nanolithography". Journal of American Chemistry Society. 125:5588 (2003).

[8] Abhijit B; Ilker SB; Alexandru SB; Tao Wang; Enkeleda D; Franz F, "Advances in top–down and bottom–up surface nanofabrication: Techniques, applications & future prospects". Advances in Colloid and Interface Science. 170: 2-27, (2012).

[9] Mohammad MA; Mustafa M; Dew SK; Stepanova M, "The Interdependence of Exposure and Development Conditions when Optimizing Low-Energy EBL for Nano-Scale Resolution In: Nanofabrication Techniques and Principles", Springer M. Stepanova and S. Dew (Eds.) 350 (2012).

[10] Madou MJ, "Fundamentals of Microfabrication: the science of miniaturization", CRC Press (2002).

[11] Wei Lu; Charles ML, "Nanoelectronics from the bottom up". Nature Materials. 6: 841 - 850 (2007)

Chapter 2

[1] Prabhakar B; Subal S; Eli Y; HyungJun K; YaHong Xie, "The fabrication of p-Ge/n-Si photodetectors, compatible with back-end Si CMOS processing, by low temperature (< 400 °C) molecular beam epitaxy and electron-beam evaporation". MRS Proceedings. 796 (2003)

[2] "Nanochrome 1 R&D Load-Lock system"- exposed by Intlvac Thin Film Corporation,

http://www.intlvac.com/products-services/thin-film-deposition-systems/r-d/nanochrome-i-ll
[3] Richard CJ, "Introduction to Microelectronic Fabrication: Volume 5 of Modular Series on Solid State Devices (2nd Edition)" Pearson Education. (2001)
[4] Woong Lee; Min-Chang Jeong; Jae-Min Myoung, "Catalyst-free growth of ZnO nanowires by metal-organic chemical vapour deposition (MOCVD) and thermal evaporation". Acta Materialia. 52: 3949–3957 (2004)
[5] "Vacuum Thermal Evaporation"- exposed by Hivatec Laboratory,
http://hivatec.ca/consulting-design/thin-film-deposition/
[6] Schiller S; Jaesch G; Nermann M, "High rate electron beam Evaporation". Thin Solid Films. 110:149-164 (1983)
[7] "A graphical representation of the selectivity of wet etching"- exposed by Wikipedia,
https://en.wikipedia.org/wiki/Etching_(microfabrication)
[8] John OD; Farooq A; Khir MH, "CMOS Compatible Bulk Micromachining". Advances in Micro/Nano Electromechanical Systems and Fabrication Technologies. ISBN 978-953-51-1085-9. Chapter 5(2013)
[9] Simon M Sze; Ming-Kwei Lee, "Semiconductor Devices: Physics and Technology". ISBN 0-471-33372-7. (2001)
[10] Bean KE, "Anisotropic etching of silicon". IEEE Transactions on Electron Devices. ED-25, 1185 (1978)
[11] Wolf S; Tauber RN, "Silicon Processing for the VLSI Era: Volume 1- Process Technology". Lattice Press. ISBN 0-9616721-3-7. 531-534 (1986)
[12] "Etchants for common microfabrication materials"- exposed by Wikipedia,
https://en.wikipedia.org/wiki/Etching_(microfabrication)
[13] "Basic Mechanism of a DC Plasma discharge"- exposed in the slide of "Application of thin films in contemporary industry".
http://www.slideshare.net/laboratoridalbasso/obst-salento-1st
[14] Faycal S; Celal C; Alanoud A; Mustafa Y; Bo Cui, "Fabrication of silicon nanostructures with large taper angle by reactive ion etching". Journal of Vacuum Science & Technology B. 32 (2014)
[15] Horiike h, Proc. 19th Semiconductor Technology Seminar, p.193 (1981)
[16] Nojiri K, "Dry Etching Technology for Semiconductors". Springer International. ISBN 978-3-319-10295-5. Chapter 2 (2015)

[17] Coburn JW; Winters HF, "Ion- and electron- assisted gas-surface chemistry- An important effect in plasma etching". Journal of Applied Physics. 50: 3189 (1979)
[18] Mogab CJ, "The loading effect of plasma etching", Journal of the Electrochemical Society. 124: 1262 (1977)
[19] Henri J; Han G; Meint de B; Miko E and Jan F, "A survey on the reactive ion etching of silicon in microtechnology", Journal of Micromechanics and Microengineering. 6:14-28(1996)

Chapter 3

[1] Bai C, "Scanning tunneling microscopy and its applications". New York: Springer Verlag. ISBN 3-540-65715-0 (2000)
[2] Binnig G; Quate CF; Gerber CH, "Atomic Force Microscope". Physical Review Letters. Vol 56: 9 (1986)
[3] Albrecht, TR.; Akamine, S; Carver, TE.; Quate, CF.; "Microfabrication of cantilever styli for the atomic force microscope". Journal of Vacuum Science & Technology A – Vacuum Surfaces and Films. 8 (4): 3386–3396 (1990)
[4] "AFM tip basics"- exposed by NanoWorld Services GmbH
https://www.agilent.com/cs/library/slidepresentation/Public/AFM%20Probe%20ManufacturingNanoworld_tip_technologyPRussell07.pdf
[5] Gerrard JP, "A Laboratory Course in Nanoscience and Nanotechnology". CRC Press. ISBN-9781482231038. Chapter 5:199 (2014)
[6] Bharat B; Othmar M, "Nanotribology and Nanomechanics I: Measurement Techniques and Nanomechanics". Springer-Verlag Berlin Heidelberg. ISBN- 978-3-642-15282-5. Chapter 2: 47-48(2011)
[7] Peter Eaton, "AFM: Beginner's Guide", www.afmhelp.com (2009)
[8] Boisen A; Rasmussen JP, Hansen O; Bouwstra S, "Indirect tip fabrication for Scanning Probe Microscopy". Microelectronic Engineering 30:579-582(1996)
[9] Olmos CM; Rasool HI; Weiller BH; Gimzewski, "Graphene MEMS: AFM probe performance improvement", ACS nano 7(5): 4164–4170 (2013)
[10] Marcus RB; Ravi TS; Gmitter T; Chin K; Liu D; Orvis WJ; Ciarlo DR; Hunt CE; Trujillo J, "Formation of silicon tips with <1 nm radius". Applied Physics Letter 56 (3): 236 (1990)
[11] Exposed by Nano Sensors.
http://www.nanosensors.com/

[12] Hafner JH; Cheung CL, Woolley AT, Lieber CM, "Structural and functional imaging with carbon nanotube AFM probes". Progress in Biophysics & Molecular Biology. 77: PP73–110 (2001)
[13] Dai H; Hafner JH; Rinzler AG; Colbert DT; Smalley RE, "Nanotubes as nanoprobes in scanning probe microscopy". Nature. 384: 147–151 (1996)
[14] Krishnan A; Dujardin E; Ebbesen TW; Yianilos PN; Treacy MM, "Young's modulus of single-walled nanotubes". Journal of Physical Review B. 58: 14013–14019 (1999)
[15] Wong EW; Sheehan PE; Lieber CM, "Nanobeam Mechanics: Elasticity, Strength, and Toughness of Nanorods and Nanotubes". Science. 277 (1997).
[16] Hafner JH; Bronikowski MJ; Azamian BR; Nikolaev P; Rinzler AG; Colbert DT; Smith K; Smalley RE, "Catalytic growth of single-wall carbon nanotubes from metal particles". Chemical Physics Letter. 296: 195–202 (1998).
[17] Hafner JH; Cheung CL; Lieber CM, "Growth of nanotubes for probe microscopy tips". Nature. 398: 761–762(1999).
[18] Hafner JH; Cheung CL; Lieber CM, "Direct growth of single-walled carbon nanotube scanning probe microscopy tips". Journal of the American Chemical Society. 121: 9750–9751(1999)

Chapter 4

[1] Calabri1 L; Pugno N; Menozzi1 C; Valeri S, "AFM nanoindentation: tip shape and tip radius of curvature effect on the hardness measurement". Journal of Physics: Condensed Matter. 20:474208-474214 (2008)
[2] Calabri L, Pugno N, Rota A, Marchetto D; Valeri S, "Nanoindentation shape-effect: experiments, simulations and modeling". Journal of Physics: Condensed Matter. 19: 395002–395013 (2007)
[3] "AFM tip by shape"- exposed by Nano and More USA,
http://www.nanoandmore.com/USA/afm-tips.php
[4] Guisbiersa G; Strehleb S; Wauteleta M, "Modeling of residual stresses in thin films deposited by electron beam evaporation". Microelectronic Engineering. 82: 665-669 (2005)
[5] Chienliu Chang; Yeong-Feng Wang; Yoshiaki Kanamori; Ji-Jheng Shih; Yusuke Kawai; Chih-Kung Lee; Kuang-Chong Wu; Masayoshi Esashi, "Etching submicrometer trenches by using the Bosch process and its application to the fabrication of antireflection structures". Journal of Micromechanics and Microengineering. 15: 580–585 (2005)

[6] Niclas Roxhed; Patrick Griss; Goran Stemme, "A method for tapered deep reactive ion etching using a modified Bosch process". Journal of Micromechanics and Microengineering. 17: 1087–1092 (2007)

[7] Martya F; Rousseaua L; Saadanya B; Merciera B; Françaisa O; Mitab Y; Bourouinaa T, "Advanced etching of silicon based on deep reactive ion etching for silicon high aspect ratio microstructures and three-dimensional micro- and nanostructures". Microelectronics Journal. 36: 673-677 (2005)

[8] Faycal S; Celal C, Alanoud A; Mustafa Y; Bo Cui, "Fabrication of silicon nanostructures with large taper angle by reactive ion etching". Journal of Vacuum Science & Technology B. 32 (2014)

Chapter 5

[1] Shuo Zheng; Ripon KD; Ferhat A; Bo Cui, "Mixture of ZEP and PMMA with varying ratios for tunable sensitivity as a lift-off resist with controllable undercut", Journal of Vacuum of Science & Technology B. 34: 06K603 (2016)

[2] Abbas AS; Alqarni S; Shokouhi BB; Yavuz M; Bo Cui, Proceedings of the 14th IEEE International Conference on Nanotechnology. 18-21 (2014)

[3] Howard RE; Hu E L; Jackel LD, "Multilevel Resist for Lithography Below 100nm", IEEE Transactions on Electron Devices. 28: 1378 (1981)

[4] Takenaka H; Todokoro Y, Proc. SPIE.1089: 132 (1989)

[5] Lihua An; Yuankai Zheng; Kebin Li; Ping Luo; Yihong Wu, "Nanometer metal line fabrication using a ZEP520 / 50KZEP520 / 50K PMMA bilayer resist by e-beam lithography", Journal of Vacuum Science & Technology B. 23: 1603 (2005)

[6] Cord B; Dames C; Berggren KK; Aumentado J, "Robust shadow-mask evaporation via lithographically controlled undercut", Journal of Vacuum of Science & Technology B. 24: 3139 (2006)

[7] Mohammad MA; Muhammad M; Dew SK; Stepanova M, Chapter 2 in Nanofabrication, edited by Stepanova M and Dew SK, Springer-Verlag/Wien (2012)

[8] Ripon KD; Bo Cui, "Lift-off with solvent for negative resist using low energy electron beam exposure", Journal of Vacuum of Science & Technology B. 32 (2014)

[9] Abbas AS; Alqarni S; Shokouhi BB; Yavuz M; Bo Cui, "Water soluble and metal-containing electron beam resist poly(sodium 4-styrenesulfonate)", Material Research Express.1 (2014)

[10] Hajiaboli AR; Bo Cui; Kahrizi M; Truong MM, "Optical properties of thick metal nanohole arrays fabricated by electron-beam and nanosphere lithography", Physica status solidi A. 206:976 (2009)

[11] Yifang Chen; Kaiwu Peng; Zheng Cui, "A lift-off process for high resolution patterns using PMMA/LOR resist stack", Microelectronic Engineering 73-74: 278 (2004)

[12] Takano H; Nakano H; Minami H; Hosogi K; Yoshida N; Sato K; Hirose Y; Tsubouchi N, "Electron-beam/ultraviolet hybrid exposure combined with novel bilayer resist system for a 0.15 μm T-shaped gate fabrication process", Journal of Vacuum of Science & Technology B. 14 (6): 3483 (1996)

[13] Bo Cui; Teodor V, "High resolution electron beam lithography of PMGI using solvent developers", Microelectronic Engineering. 85: 810 (2008)

[14] Yan M; Choi S; Subramanian KRV; Adesida I, "The effects of molecular weight on the exposure characteristics of poly(methylmethacrylate) developed at low temperatures", Journal of Vacuum of Science & Technology B. 26:2306 (2008)

[15] Maximov I; Sarwe EL; Beck M; Deppert K; Graczyk M; Magnusson MH; Montelius L, "Fabrication of Si-based nanoimprint stamps with sub-20 nm features", Microelectronic Engineering. 61-62:449 (2002)

[16] Ishii T; Tanaka H; Kuramochi E; Tamamura T, "Fabrication of Nanometer-Order Dot Patterns by Lift-off Using a Fullerene-Incorporated Bilayer Resist System", Japanese Journal of Applied Physics. 37: 7202 (1998)

[17] Haifang Yang; Aizi Jin; Qiang Luo; Junjie Li; Changzhi Gu; Zheng Cui, "Electron beam lithography of HSQ/PMMA bilayer resists for negative tone lift-off process", Microelectronic Engineering. 85: 814-817 (2007)

[18] Ma S; Con C; Yavuz M; Bo Cui, "Polystyrene Negative Resist for High Resolution Electron Beam Lithography", Nanoscale Research Letter. 6:446 (2011)

[19] Con C; Dey R; Ferguson M; Zhang J; Mansour R; Yavuz M; Bo Cui, "High molecular weight polystyrene as very sensitive electron beam resist", Microelectronic Engineering. 98: 254-257(2012)

[20] Dey RK; Mansour R; Bo Cui, "Effect of molecular weight distribution on e-beam exposure properties of polystyrene". Nanotechnology. 24: 245302 (2013)

[21] Potyrailo RA; Bonam PK; Hartley JG et al, "Towards outperforming conventional sensor arrays with fabricated individual photonic vapour sensors inspired by Morpho butterflies", Nature Communications. 6: 7959 (2015)

[22] Rahman SMS; Bo Cui, "Mold Fabrication for 3D Dual Damascene Imprinting", Nanoscale Research Letters. 5: 545–549 (2010)